



HAL
open science

Molecular determinants for the strictly compartmentalized expression of kainate receptors in CA3 pyramidal cells

Sabine Fièvre, Mario Carta, Ingrid Chamma, Virginie Labrousse, Olivier Thoumine, Christophe Mulle

► **To cite this version:**

Sabine Fièvre, Mario Carta, Ingrid Chamma, Virginie Labrousse, Olivier Thoumine, et al.. Molecular determinants for the strictly compartmentalized expression of kainate receptors in CA3 pyramidal cells. *Nature Communications*, 2016, 7, pp.12738. <10.1038/ncomms12738>. <hal-04675006>

HAL Id: hal-04675006

<https://hal.science/hal-04675006v1>

Submitted on 22 Aug 2024

HAL is a multi-disciplinary open access archive for the deposit and dissemination of scientific research documents, whether they are published or not. The documents may come from teaching and research institutions in France or abroad, or from public or private research centers.

L'archive ouverte pluridisciplinaire **HAL**, est destinée au dépôt et à la diffusion de documents scientifiques de niveau recherche, publiés ou non, émanant des établissements d'enseignement et de recherche français ou étrangers, des laboratoires publics ou privés.



HAL Authorization

ARTICLE

Received 2 Nov 2015 | Accepted 28 Jul 2016 | Published 27 Sep 2016

DOI: 10.1038/ncomms12738

OPEN

Molecular determinants for the strictly compartmentalized expression of kainate receptors in CA3 pyramidal cells

Sabine Fièvre^{1,*}, Mario Carta^{1,*}, Ingrid Chamma¹, Virginie Labrousse¹, Olivier Thoumine¹ & Christophe Mulle¹

Distinct subtypes of ionotropic glutamate receptors can segregate to specific synaptic inputs in a given neuron. Using functional mapping by focal glutamate uncaging in CA3 pyramidal cells (PCs), we observe that kainate receptors (KARs) are strictly confined to the post-synaptic elements of mossy fibre (mf) synapses and excluded from other glutamatergic inputs and from extrasynaptic compartments. By molecular replacement in organotypic slices from GluK2 knockout mice, we show that the faithful rescue of KAR segregation at mf-CA3 synapses critically depends on the amount of GluK2a cDNA transfected and on a sequence in the GluK2a C-terminal domain responsible for interaction with N-cadherin. Targeted deletion of N-cadherin in CA3 PCs greatly reduces KAR content in thorny excrescences and KAR-EPSCs at mf-CA3 synapses. Hence, multiple mechanisms combine to confine KARs at mf-CA3 synapses, including a stringent control of the amount of GluK2 subunit in CA3 PCs and the recruitment/stabilization of KARs by N-cadherins.

¹Interdisciplinary Institute for Neuroscience, CNRS UMR 5297, University of Bordeaux, 146 rue Léo-Saignat, F-33076 Bordeaux, France. * These authors contributed equally to this work. Correspondence and requests for materials should be addressed to C.M. (email: christophe.mulle@u-bordeaux.fr).

There is an extreme anatomical and functional diversity of synapses connecting different populations of neurons. The segregation of different excitatory connections onto a single neuron is particularly striking in laminated structures such as the hippocampus¹. CA3 pyramidal cells (PCs) receive three types of glutamatergic inputs, which are precisely positioned along apical and basal dendrites, from the entorhinal cortex (perforant path), from recurrent CA3 collaterals (associational/commissural, A/C fibres) and from the dentate gyrus (DG) through mossy fibres (mf). Glutamatergic synapses from these different inputs greatly vary in their structural and functional properties. Mf inputs make synaptic contacts on proximal dendrites (PDs) of CA3 PCs (in the stratum lucidum) via 'giant' mf boutons with multiple glutamate release sites facing large postsynaptic structures called thorny excrescences (TEs)². In contrast A/C and perforant path synapses are of the single site/single spine type. Mf-CA3 synapses display a wide dynamic range of short-term plasticity and express NMDA (*N*-methyl-D-aspartate) receptor-independent presynaptic forms of long-term depression (LTD) and long-term potentiation (LTP)³.

The different families of ionotropic glutamate receptors (iGluRs), AMPA (α -amino-3-hydroxy-5-methyl-4-isoxazole propionic acid) receptors (AMPA), NMDA receptors and kainate receptors (KARs) exist as multiple subtypes endowed with distinctive properties^{4,5}. The subcellular segregation of KARs in CA3 PCs provides a striking example of synaptic specification within a single neuronal population. KARs are tetrameric iGluRs composed of combinations of five subunits GluK1–GluK5. KARs regulate the activity of synaptic circuits at presynaptic and postsynaptic sites, through either ionotropic or metabotropic actions^{6–8}. KARs are expressed and functional in principal neurons of CA1, DG and CA3, as well as in interneurons⁹. However, postsynaptic KARs activated by synaptic release of glutamate has only been encountered in CA1 interneurons and in CA3 PCs. In CA3 PCs, stimulation of mf inputs but not of A/C inputs evokes excitatory post-synaptic currents (EPSCs) mediated by KARs (KAR-EPSCs), which contain the GluK2 subunit^{10,11}. In addition, puff application of glutamate above the stratum lucidum, but not the stratum radiatum, activates KAR-mediated inward currents¹⁰. This segregation of KARs in the stratum lucidum is further supported by kainate-binding studies and by immunocytochemical labelling of GluK2 and GluK5, although these methods do not discriminate between pre- and postsynaptic KARs^{12,13}. A precise evaluation of the subcellular localization of native KARs in CA3 PCs is made difficult by the lack of high-quality antibodies.

The molecular mechanisms underlying subcellular trafficking of KARs have been explored in heterologous systems and in dissociated neuronal cultures^{6,7}, albeit in conditions that do not reproduce the strict subcellular segregation observed for native KARs in an *in vivo* situation. The subcellular trafficking and localization of neurotransmitter receptors in neurons are tightly regulated by association with interacting proteins. KAR subunits interact through their cytoplasmic carboxy-terminal domain (CTD) with a large array of proteins involved in the regulation of trafficking to the plasma membrane^{14–17}. In addition, NETO1 and NETO2 (neuropilin tolloid-like 1 and 2) act as auxiliary proteins assembling with KARs to control gating and pharmacology^{18–23}. NETO1 contributes to postsynaptic KARs at mf-CA3 synapses^{20,22}, but the effect of NETO proteins on KAR targeting is unclear^{19,24}. NETO proteins do not appear to be responsible for the segregation of KARs to mf-CA3 synapses²³. N-cadherin, which participates in transsynaptic complexes to ensure the adhesion between synaptic membranes and organize the underlying multiprotein complex²⁵, interacts with GluK2a

through its CTD domain¹⁶. In transfected heterologous cell lines, activation of N-cadherins by ligand-covered latex beads recruits GluK2 to N-cadherin/ β -catenin complexes¹⁶. Whether this interaction plays a role in the trafficking and stabilization of KARs at synaptic sites has not yet been explored.

Here we investigated the mechanisms underlying the confined subcellular expression of KARs in CA3 PCs. Both cell autonomous mechanisms and signals from afferent mfs through transsynaptic-synaptic signalling may be at play. We have used focal glutamate uncaging combined with electrophysiology to precisely characterize the functional expression of KARs and combined this functional approach with a semi-quantitative gene replacement strategy to identify molecular mechanisms for the subcellular segregation of KARs in CA3 PCs.

Results

Functional mapping of KARs in CA3 PCs. To address the molecular mechanisms underlying the compartmentalized expression of KARs in CA3 PCs, we used organotypic slice cultures as an *in vitro* system easily amenable to genetic manipulation in single identified neurons²⁶. We first compared the functional expression of KARs in acute and in organotypic slices. Minimal stimulation of mfs evoked EPSCs in CA3 PCs, which are substantially blocked by LY303070 (25 μ M), a selective antagonist of AMPARs. In both acute and cultured slices, the remaining synaptic current represented KAR-EPSCs, which were abolished in slices from GluK2^{-/-} mice (Fig. 1a–c). In both acute and organotypic slices, KAR-EPSCs can be evoked by stimulation of mfs, but not of A/C fibres (Fig. 1b,c). The KAR/AMPA ratio is comparable between the two conditions (mf KAR/AMPA ratio, acute GluK2^{+/+}: 13.2 \pm 1.1%; organotypic GluK2^{+/+}: 12.4 \pm 2.4%; acute GluK2^{-/-}: 2.3 \pm 0.2%; organotypic GluK2^{-/-}: 1.7 \pm 0.1%; A/C KAR/AMPA ratio: acute GluK2^{+/+}: 2.0 \pm 0.5%; organotypic GluK2^{+/+}: 0.1 \pm 0.0%; Fig. 1c).

KARs are strictly segregated at mf-CA3 PCs synapses and are absent from A/C inputs in organotypic slices, hence validating the model to study the mechanisms underlying synapse-specific segregation of KARs. To get a more precise evaluation of the subcellular segregation of KARs, we mapped functional KARs in single CA3 PCs using focal photolysis of caged MNI-glutamate (500 μ M) using 2 ms pulses of a 405 nm laser²⁷. Three days before recording, CA3 PCs were transfected by single-cell electroporation with a complementary DNA expressing green fluorescent protein (GFP) to reveal dendritic morphology of CA3 PCs. The output of the laser filled the back of the objective lens by 90%, to generate a minimal spot of \sim 1 μ m in the objective focal plane. The minimal laser spot formed at the focus can be seen in 100 μ M pyranine solution viewed with the charge-coupled device camera²⁷. The laser spot was positioned in three dimensions in reference to the distinct compartments of CA3 PCs. We evaluated the precision of the method by moving the laser spot at different distances away from a dendrite in the stratum radiatum, while recording AMPAR-mediated currents evoked by glutamate uncaging (Supplementary Fig. 1a,b). This provided an estimation for the spatial precision of glutamate uncaging of roughly 5–10 μ m in diameter, probably corresponding to the range of glutamate diffusion following photolysis.

We then mapped AMPARs and KARs in distinct compartments of CA3 PCs in organotypic slices (Fig. 1d). In CA3 PCs recorded in the voltage-clamp mode, glutamate uncaging evoked AMPAR-mediated currents in the soma, TEs, and proximal shaft and distal dendrites (Fig. 1e,f). Uncaging on distal dendrites included dendritic shaft and spines, whereas the spot for uncaging on the proximal shaft was positioned to avoid TEs. In striking contrast, KAR currents (in the presence of LY303070 and D-AP5)

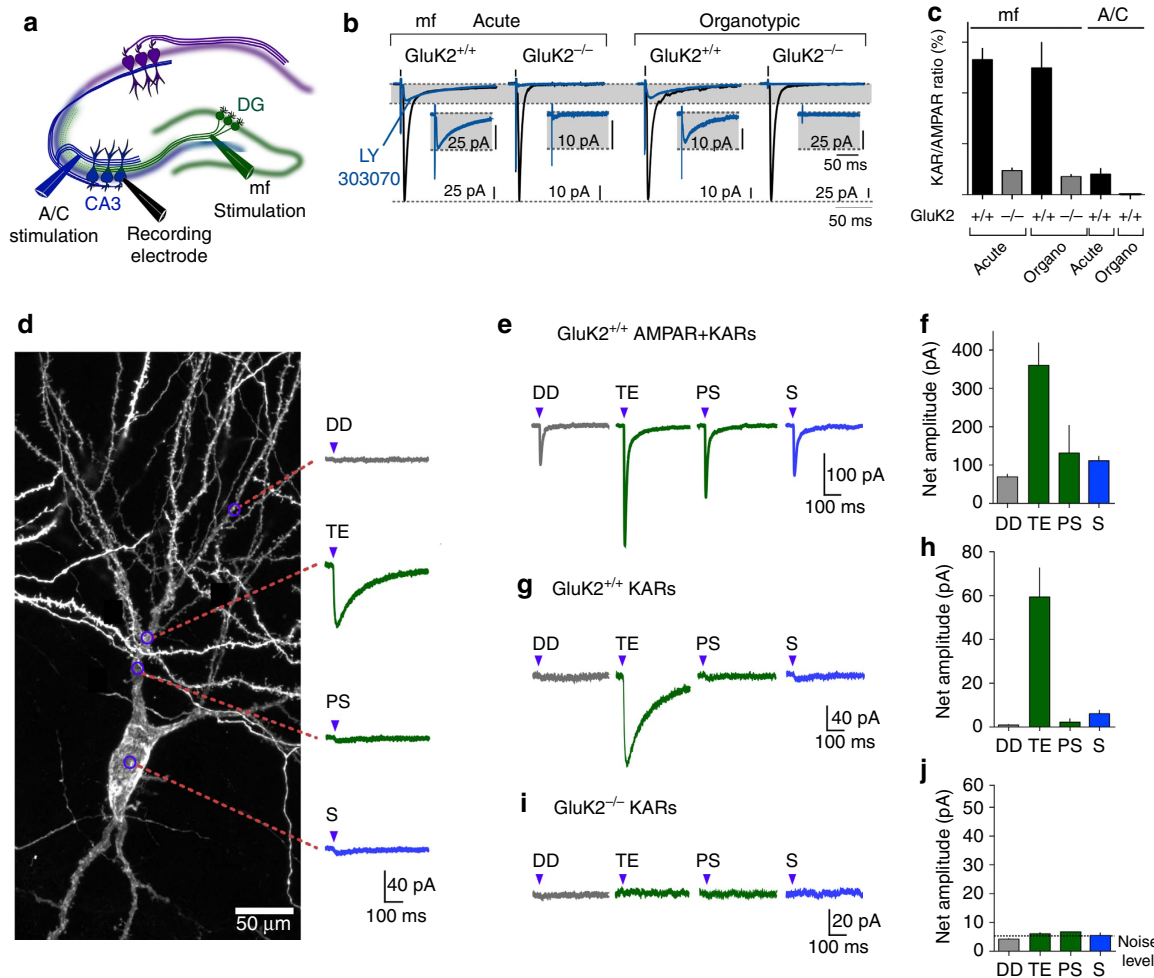


Figure 1 | Compartmentalized expression of KARs in CA3 PCs. (a) Schematic experimental setting. (b) Voltage-clamp recordings performed on CA3 PCs from acute and organotypic slices prepared from *GluK2*^{+/+} and *GluK2*^{-/-} mice, in the presence of bicuculline (10 μM), D-AP5 (50 μM) and a low concentration of NBQX (150 nM), to limit polysynaptic activity. In all, average of 30 responses evoked at 3 Hz in the absence and in the presence of 25 μM LY303070, to isolate the mf-CA3 AMPAR-EPSCs and KAR-EPSCs, respectively. Insert, enlargements of isolated KAR-EPSCs. (c) Summary graphs for the relative amplitude of KAR-EPSCs versus AMPAR-EPSCs obtained in acute and organotypic slices prepared from *GluK2*^{+/+} and *GluK2*^{-/-} mice. Mf KAR/AMPA ratio, acute *GluK2*^{+/+}: *n* = 6 cells; organotypic *GluK2*^{+/+}: *n* = 8 cells; acute *GluK2*^{-/-}: *n* = 5 cells; organotypic *GluK2*^{-/-}: *n* = 12 cells; A/C KAR/AMPA ratio: acute *GluK2*^{+/+}: *n* = 7 cells; organotypic *GluK2*^{+/+}: *n* = 7 cells; 27 mice. (d) Confocal image of a CA3 PC transfected with GFP illustrating glutamate uncaging spots (MNI glutamate, 500 μM) and corresponding evoked KAR currents. Purple arrowheads represent time of uncaging (405 nm, 2 ms). Average of five responses evoked at 0.1 Hz at each uncaging site. (e,f) Sample traces illustrating currents evoked by glutamate uncaging (bicuculline 10 μM, D-AP5 50 μM and NBQX 150 nM) in *GluK2*^{+/+} organotypic slices in different compartments of CA3 PCs, soma (S), thorny excrescences (TE), proximal shaft (PS) and distal dendrites (DDs). Summary graph of the average of net amplitude of evoked currents. Uncaging sites: S, *n* = 3; TE, *n* = 7; PS, *n* = 3; DD, *n* = 10, from 4 cells; 2 mice. (g,h) Sample traces illustrating KAR currents evoked by glutamate uncaging in *GluK2*^{+/+} organotypic slices in different compartments of CA3 PCs. Graph summarizing the average net amplitude of evoked KAR currents. Uncaging sites: S, *n* = 7; TE, *n* = 10; PS, *n* = 5; DD, *n* = 10, from 10 cells; 6 mice. (i,j) Sample traces illustrating the lack of KAR currents evoked by glutamate uncaging in *GluK2*^{-/-} organotypic slices in different compartments of CA3 PCs. Graph summarizing the average net amplitude of the evoked currents. Uncaging sites: S, *n* = 8; TE, *n* = 18; PS, *n* = 1; DD, *n* = 8, from 5 cells; 4 mice.

could only be evoked when the uncaging spot was localized above visually identified TEs (average amplitude 59.4 ± 13.2 pA, *n* = 10; Fig. 1g,h). No KAR current could be evoked when the laser spot was either positioned on the soma, on the shaft of PDs or on DDs. No KAR current was evoked in *GluK2*^{-/-} organotypic slices (Fig. 1i,j) or in any compartment of CA1 PCs (Fig. 1d,e), further indicating that all other iGluRs were adequately blocked. In acute slices, functional mapping of KARs revealed a similar restricted pattern of expression (Supplementary Fig. 1f,g). These functional mapping results highlight a clear distinction between iGluR subtypes. AMPARs are readily expressed at synaptic and extrasynaptic sites, that is, on the soma and dendritic shafts. In contrast, KARs appear excluded from the soma and from the

proximal and distal dendritic shafts, and are only activated when the laser is focused on TEs. With the current resolution of laser uncaging we cannot exclude the presence of KARs at perisynaptic sites within the TE, given the small spacing (300–400 nm) between the different postsynaptic densities (PSDs)^{28,29}.

Semi-quantitative replacement of *GluK2* in *GluK2*^{-/-} mice. To gain insight into the mechanism of compartmentalization of KARs in CA3 PCs, we used a molecular substitution approach in combination with slice electrophysiology and glutamate uncaging (Fig. 2). In slices prepared from *GluK2*^{-/-} mice, glutamate uncaging on TEs of CA3 PCs did not evoke any detectable

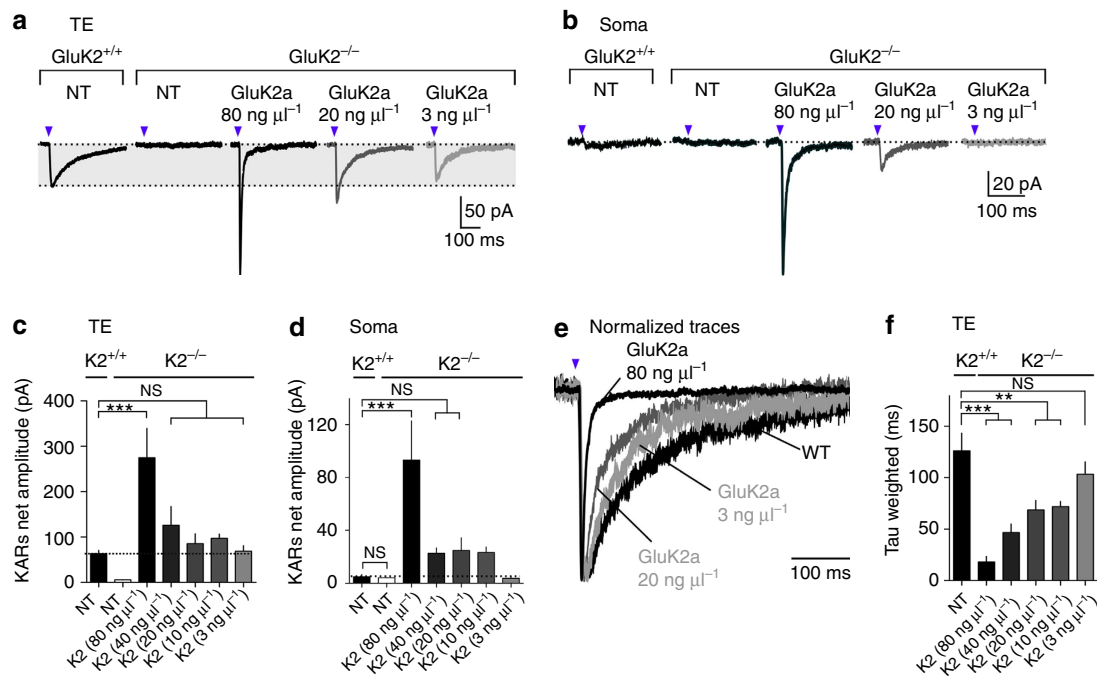


Figure 2 | Semi-quantitative replacement of KARs. (a,b) Sample traces illustrating KAR currents evoked by glutamate uncaging on TEs (a) and soma (b) of CA3 PCs in organotypic slice cultures prepared from GluK2^{+/+} and GluK2^{-/-} mice not transfected (NT) or transfected with different amounts of GluK2a cDNA (80, 20 and 3 ng μl⁻¹). (c,d) Bar graphs summarizing the average amplitude of KAR currents evoked by glutamate uncaging on TEs (c) or on the soma (d) in the different conditions (mean amplitude per cell). GluK2^{+/+} NT: *n* = 22; GluK2^{-/-} NT: *n* = 11; 80 ng μl⁻¹: *n* = 14; 40 ng μl⁻¹: *n* = 6; 20 ng μl⁻¹: *n* = 11; 10 ng μl⁻¹: *n* = 12; 6 ng μl⁻¹: *n* = 7; 3 ng μl⁻¹: *n* = 16; 43 mice. (e,f) Sample traces of KAR currents evoked by glutamate uncaging shown in a and scaled at the peak illustrating differences in the decay kinetics for various conditions. (f) Quantification of the decay rate (tau weighted) of KAR currents evoked by glutamate uncaging for the different conditions. GluK2^{+/+} NT: *n* = 7; 80 ng μl⁻¹: *n* = 7; 40 ng μl⁻¹: *n* = 6; 20 ng μl⁻¹: *n* = 10; 10 ng μl⁻¹: *n* = 12; 6 ng μl⁻¹: *n* = 8; 3 ng μl⁻¹: *n* = 6; 43 mice. In all panels, values are presented as mean ± s.e.m. of *n* experiments. Data were compared using one-way analysis of variance followed by Dunnett's multiple comparison test (NS, not significant; *P* > 0.05, ***P* < 0.01 and ****P* < 0.001).

current, as expected. We then rescued functional KARs in GluK2^{-/-} slices using single-cell electroporation of CA3-PCs. A main advantage of single-cell electroporation, with respect to viral infection, is the possibility to control the amount of cDNA transfected, in addition to being able to precisely target CA3 PCs. We transfected various concentrations (3, 10, 20, 40 and 80 ng μl⁻¹) of cDNA encoding GluK2a together with cDNA encoding soluble GFP as a reporter (Fig. 2 and Supplementary Fig. 2). Two to 3 days after electroporation of GluK2a cDNA at a concentration as low as 3 ng μl⁻¹, KAR currents evoked by focal glutamate uncaging onto TEs could be successfully recorded. The amplitude of KAR currents depended on the amount of cDNA transfected (mean amplitude: 80 ng μl⁻¹: 275.2 ± 64.4 pA; 40 ng μl⁻¹: 126.1 ± 41.3 pA; 20 ng μl⁻¹: 85.3 ± 22.1 pA; 10 ng μl⁻¹: 97.3 ± 9.5 pA; 3 ng μl⁻¹: 68.7 ± 12.3 pA; Fig. 2a–c). The average amplitude of native KAR currents in wild-type (WT) slices corresponded best to the lowest concentration of GluK2a cDNA (3 ng μl⁻¹). Importantly, with higher GluK2a cDNA concentrations, aberrant KAR currents were also evoked with focal glutamate uncaging onto the soma (Fig. 2b–d) and DDs (Supplementary Fig. 2), in stark contrast with the native situation (soma, mean amplitude: 80 ng μl⁻¹: 93.2 ± 29.7 pA; 40 ng μl⁻¹: 22.8 ± 4.1 pA; 20 ng μl⁻¹: 24.9 ± 9.6 pA; 10 ng μl⁻¹: 23.3 ± 4.2 pA).

In WT slices, KAR currents displayed slow decay kinetics (mean tau-weighted WT: 126 ± 17 ms), as a probable consequence of the heteromeric composition of native KARs and interaction with auxiliary subunits such as NETOs^{18,20,30–32}. In CA3 PCs of GluK2^{-/-} mice transfected with GluK2a cDNA, the decay kinetics of KAR currents evoked by focal glutamate

uncaging onto TEs was much faster than in native conditions for concentrations GluK2a cDNA of 10 ng μl⁻¹ and above (mean tau-weighted GluK2a 80 ng μl⁻¹: 18.1 ± 5.5 ms; 40 ng μl⁻¹: 46.6 ± 8.6 ms; GluK2a 20 ng μl⁻¹: 68.6 ± 9.4 ms; GluK2a 10 ng μl⁻¹: 71.9 ± 5.1 ms; Fig. 2e,f). The electroporation of 3 ng μl⁻¹ GluK2a cDNA restored decay kinetics to values not significantly different from WT (mean tau-weighted GluK2a 3 ng μl⁻¹: 103.4 ± 12.0 ms). In addition, KAR currents evoked in the soma for concentrations of GluK2a cDNA of 10 ng μl⁻¹ and above also displayed fast decay kinetics (mean tau-weighted GluK2a 80 ng μl⁻¹: 16.2 ± 2.1 ms). From a methodological standpoint, these semi-quantitative re-expression experiments clearly show that the amount of cDNA transfected and, consequently, of GluK2a protein is critical for a faithful rescue of KAR subcellular segregation similar to native conditions. The use of a low amount of GluK2a cDNA (3 ng μl⁻¹) restored the restricted functional expression of KARs in TEs, whereas transfection of a higher amount of cDNA led to the functional expression of KARs with ectopic localization and aberrant kinetics.

Recombinant homomeric GluK2 KARs display notably faster deactivation kinetics than heteromeric GluK2/GluK5 when activated by a short (1 ms) pulse of glutamate³¹. Fast decay kinetics of ectopic KAR currents observed in conditions of overexpression of GluK2 may be due to a prevalence of homomeric GluK2. To test this hypothesis, we used UBP310 as an antagonist of recombinant heteromeric GluK2/GluK5 KARs and synaptic KARs, which spares homomeric GluK2 KARs³³. We observed that in WT slices, KAR currents evoked by glutamate uncaging on TEs was strongly inhibited by 3 μM UBP310 (mean

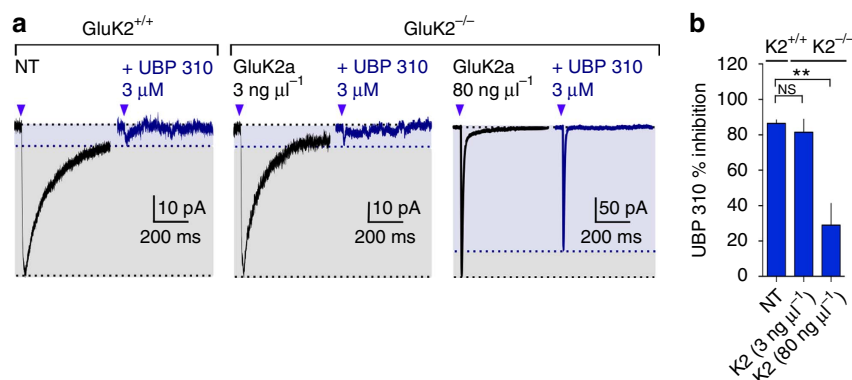


Figure 3 | Block of KAR currents by the GluK2/GluK5 antagonist UBP310. (a) Sample traces illustrating KAR currents evoked by glutamate uncaging on TEs of CA3 PCs in organotypic slice cultures prepared from GluK2^{+/+} and GluK2^{-/-} not transfected (NT) or transfected with 3 ng μl⁻¹ of GluK2a cDNA or 80 ng μl⁻¹ in the absence or presence of UBP 310 (3 μM). (b) Bar graph summarizing the percentage of inhibition of UBP 310 (3 μM) on the KAR currents evoked by glutamate uncaging. In GluK2^{+/+} NT: $n = 6$ cells; 3 ng μl⁻¹: $n = 7$ cells; 3 ng μl⁻¹: $n = 12$ cells; 7 mice. Values are presented as mean ± s.e.m. of n experiments. Data were compared using one-way analysis of variance followed by Dunnett's multiple comparison test (NS, not significant; $P > 0.05$ and $**P < 0.01$).

% of inhibition: $86.5 \pm 2.0\%$; Fig. 3) confirming that native KARs in CA3 PCs are likely to be heteromeric KARs. In CA3 PCs from GluK2^{-/-} mice, following transfection of low concentrations of GluK2 cDNA (3 ng μl⁻¹), KARs were also largely inhibited by UBP310 (mean % of inhibition: $81.6 \pm 7.4\%$; Fig. 3). In contrast, following transfection of a higher amount of cDNA (80 ng μl⁻¹), inhibition of KAR currents evoked by glutamate uncaging on TEs was largely attenuated (mean % of inhibition: $29.0 \pm 12.3\%$) and this inhibition spared the fast decaying component of the response (Fig. 3). These results strongly suggest that following transfection of a high concentration of GluK2a cDNA, ectopic KARs with fast decay kinetics represent a pool of homomeric GluK2 KARs. These experiments also strongly support the notion that native KARs are heteromeric KARs. KAR currents can be successfully rescued in CA3-PCs albeit faithful replacement of KARs in CA3 PCs requires transfection of precise amounts of GluK2a cDNA.

Synaptic rescue of KARs in GluK2^{-/-} mice. We then attempted to selectively rescue synaptic KARs at mf-CA3 synapses in GluK2^{-/-} slices. AMPAR- and KAR-mediated EPSCs were evoked by electrical stimulation of mf and A/C inputs to CA3 PCs (Fig. 4a–c). To normalize the intrinsic variability at mf-CA3 synapses, the relative amplitude of KAR-EPSCs was measured with respect to the amplitude of AMPAR-EPSCs for each cell recorded, as previously described²⁶. KAR-EPSCs could be rescued at mf-CA3 synapses with concentrations of GluK2a cDNA of 3 ng μl⁻¹ and above. Interestingly, the KAR/AMPA ratio was comparable to WT for all concentrations of cDNA electroporated (KAR/AMPA ratio, WT: $10.8 \pm 2.1\%$; GluK2^{-/-} not transfected: $0.8 \pm 0.1\%$; 80 ng μl⁻¹: $11.2 \pm 1.2\%$; 20 ng μl⁻¹: $9.9 \pm 1.0\%$; 10 ng μl⁻¹: $8.5 \pm 1.2\%$; 3 ng μl⁻¹: $9.5 \pm 0.8\%$; $P > 0.05$; Fig. 4c). Stimulation of A/C inputs did not elicit any KAR-EPSCs neither in WT slices nor in GluK2^{-/-} CA3 PCs transfected with high concentration of GluK2a cDNA (A/C KAR/AMPA ratio, WT: $0.1 \pm 0.0\%$; GluK2a 80 ng μl⁻¹: $0.1 \pm 0.1\%$; Student's t -test; $P > 0.05$). The decay kinetics of KAR-EPSCs were not statistically different between WT and GluK2^{-/-} conditions with various amount of GluK2a cDNA electroporated (mean tau-weighted WT: 49.9 ± 7.0 ms; GluK2 80 ng μl⁻¹: 32.4 ± 8.6 ms; 20 ng μl⁻¹: 31.5 ± 2.6 ms; 10 ng μl⁻¹: 42.6 ± 8.9 ms; 3 ng μl⁻¹: 41.0 ± 7.8 ms; $P > 0.05$; Fig. 4d,e). Thus, synaptically evoked KARs were reliably rescued at mf-CA3 synapses and were absent from

other inputs, mimicking the distribution of native KARs. In addition, whereas the use of high cDNA concentration led to the expression of ectopic extrasynaptic KAR currents of large amplitude, the relative amplitude of KAR-EPSCs did not differ between the different concentrations of cDNA. Although the content of synaptic KARs is precisely controlled independently of the copy number of GluK2a cDNA expressed, the amount of extrasynaptic KARs depends on the concentration of cDNA electroporated. These observations imply that at synaptic contacts an active and specific molecular machinery precisely regulates the amount of KARs, possibly due to a limited number of slots to accommodate synaptic KARs at mf-CA3 synapses.

Subcellular imaging of recombinant GluK2a in CA3-PCs.

Visualization of subcellular distribution of KARs neurons is limited by the lack of good antibodies. To circumvent this issue, we expressed GluK2a subunits bearing an amino-terminal SEP tag³⁴ in CA3-PCs and labelled them with anti-GFP nanobodies conjugated to photostable organic dyes³⁵. These small ligands (~3 nm) show rapid penetration into thick organotypic tissue in live conditions³⁶, allowing robust staining of surface SEP–GluK2a. Specifically, we electroporated SEP–GluK2a at cDNA concentrations of 3 or 80 ng μl⁻¹ in CA3 PCs of GluK2^{-/-} slices, thus replacing endogenous KARs by SEP–GluK2a. KAR currents evoked by focal glutamate uncaging after expression of SEP–GluK2a (3 and 80 ng μl⁻¹) were of similar amplitudes as that observed when GluK2a-WT was expressed (Supplementary Fig. 3). Moreover, mf-CA3 synaptic KARs were faithfully rescued after electroporation of SEP–GluK2a (3 ng μl⁻¹ cDNA; Supplementary Fig. 3). When 3 ng μl⁻¹ cDNA concentration was used, SEP–GluK2 clusters detected by confocal microscopy were selectively localized at TEs and were barely detectable in the soma or in DDs (number of clusters per μm length; 3 ng μl⁻¹: soma, 0.027 ± 0.012 ; TE, 0.19 ± 0.045 ; DD, 0.03 ± 0.036 ; Fig. 5a,b). In contrast, at high cDNA concentration (80 ng μl⁻¹), SEP–GluK2 clusters were abundant in both the soma and DDs, although the highest levels were again detected at TEs (number of clusters per μm length; 80 ng μl⁻¹: soma, 0.132 ± 0.036 ; TE, 0.436 ± 0.097 ; DD, 0.215 ± 0.023 ; Fig. 5a,b). Overall, these morphological data corroborate the functional subcellular distribution of KARs and confirm that aberrant ectopic KARs are expressed when a high concentration of cDNA is used.

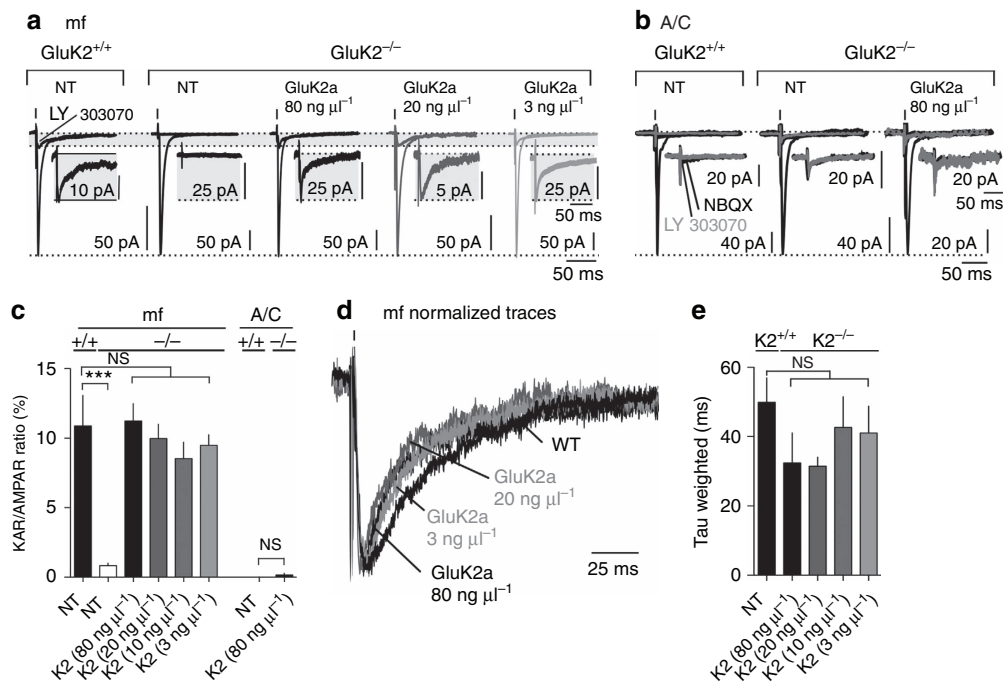


Figure 4 | Rescue of synaptic KARs at mf-CA3 synapses. (a,b) Sample traces illustrating synaptic currents evoked by mf stimulation (a) and A/C stimulation (b) in organotypic slices prepared from GluK2^{+/+} and GluK2^{-/-} mice, not transfected (NT) or transfected with different amounts of GluK2a cDNA (80, 20 and 3 ng μl⁻¹). Experiments were performed in the presence of bicuculline (10 μM), D-AP5 (50 μM) and NBQX (150 nM). Traces represent the average of synaptic currents evoked at 3 Hz in the absence and in the presence of 25 μM LY303070, to isolate the AMPAR and the KAR component, respectively. In the insert are shown enlargements, by the same proportion, of isolated KAR-EPSCs. (c) Bar graph summarizing the KAR/AMPA ratio obtained from the experiments presented in a and b. Mf stimulation: GluK2^{+/+} NT: *n* = 7 cells; GluK2^{-/-} NT: *n* = 10 cells; 80 ng μl⁻¹: *n* = 6 cells; 20 ng μl⁻¹: *n* = 9 cells; 10 ng μl⁻¹: *n* = 7 cells; 3 ng μl⁻¹: *n* = 9 cells. A/C stimulation: GluK2^{+/+} NT: *n* = 9 cells; 80 ng μl⁻¹: *n* = 6 cells; 32 mice. (d,e) Sample traces of mf-CA3 KAR-EPSCs shown in a and scaled at the peak illustrating the lack of difference in the decay kinetics for various conditions. (e) Quantification of the decay rate (tau weighted) of KAR-EPSCs from cells transfected with different amount of cDNA encoding for GluK2a. In all panels, values are presented as mean ± s.e.m. of *n* experiments. In c, data were compared using one-way analysis of variance followed by Dunnett's multiple comparison test, except for A/C experiments that were compared with an unpaired *t*-test (NS, not significant; *P* > 0.05 and ****P* < 0.001).

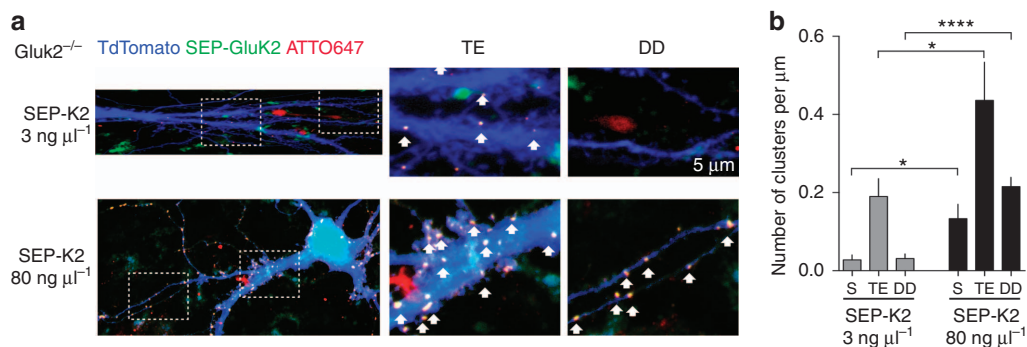


Figure 5 | Subcellular distribution of SEP-GluK2a in CA3 PCs. (a) Sample images illustrating CA3 neurons electroporated with 3 ng μl⁻¹ (top) or 80 ng μl⁻¹ (bottom) SEP-GluK2 cDNA (green), TdTomato (blue) and live stained for the SEP moiety using anti-GFP nanobody-ATTO647 (red). Representative confocal z-stack projections are shown for each condition. Insets represent characteristic CA3 TEs or DDs. Arrows show the co-localized SEP and anti-GFP nanobody signals that correspond to SEP-GluK2 clusters. (b) Average number of clusters per unit length at the soma (S), TE or DD for each condition (3 ng μl⁻¹: *n* = 11 cells, 3 different experiments, 3 mice; 80 ng μl⁻¹: *n* = 10 cells, 3 different experiments, 3 mice). In all panels, values are presented as mean ± s.e.m. of *n* experiments. Data were compared using unpaired *t*-test (**P* < 0.05 and *****P* < 0.0001).

GluK2a C terminus stabilizes KARs at mf-CA3 synapses. The CTD of GluK2 is the target of multiple proteins that modulate the trafficking of KARs to the plasma membrane^{6,15,37–39}. We studied the role of the CTD of GluK2a in the stabilization of KARs at mf-CA3 synapses by reexpressing different truncated forms of GluK2a subunits in CA3 PCs in organotypic slices of GluK2^{-/-} mice (Fig. 6). The cDNAs (3 ng μl⁻¹) coding for different GluK2a subunits truncated in the CTD (GluK2aΔ4;

GluK2aΔ14; GluK2aΔ29 and GluK2aΔ39) were electroporated in CA3 PCs (Fig. 6a). AMPAR- and KAR-EPSCs were evoked by mf electrical stimulation (Fig. 6b,c). Re-expression of GluK2aΔ4, a GluK2a subunit lacking the PDZ domain-binding motif necessary for the interaction with PSD95, rescued KAR-EPSCs with a relative amplitude comparable to WT (KAR/AMPA ratio WT: 10.0 ± 1.3%; GluK2aΔ4: 9.7 ± 1.4%), suggesting that this molecular interaction is not critical for the retention of KARs

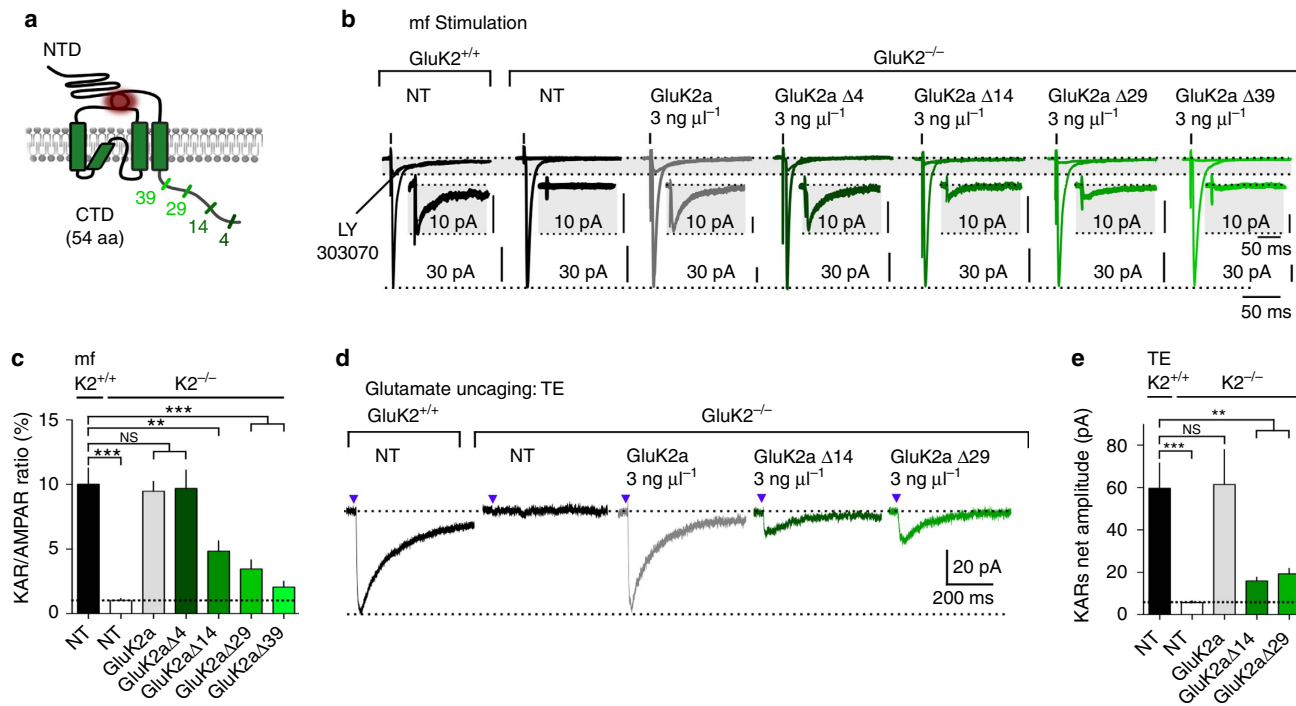


Figure 6 | GluK2a C-terminal sequence is necessary for stabilization of synaptic KARs. (a) Schematic representation of the GluK2a subunit, illustrating the sites at which the CTD was truncated. (b,c) Sample traces illustrating synaptic currents evoked by mf stimulation in organotypic slices prepared from GluK2^{+/+} and GluK2^{-/-} mice, not transfected (NT) or transfected with 3 ng μl⁻¹ of wt or mutated GluK2a cDNA (Δ4, Δ14, Δ29 and Δ39). Experiments were performed in the presence of bicuculline (10 μM), D-AP5 (50 μM) and NBQX (150 nM). Traces represent the average of synaptic currents evoked at 3 Hz in the absence and in the presence of 25 μM LY303070, to isolate the AMPAR and the KAR component, respectively. In the insert are shown enlargements, by the same proportion, of isolated KAR-EPSCs. (c) Bar graphs summarizing KAR/AMPA ratios obtained from the experiments presented in b. GluK2^{+/+} NT: n = 8 cells; GluK2^{-/-} NT: n = 8; GluK2^{-/-} + GluK2a: n = 9 cells; GluK2Δ4: n = 12 cells; GluK2Δ14: n = 7 cells; GluK2Δ29: n = 12 cells; GluK2Δ39: n = 8 cells. 40 mice. (d,e) Sample traces illustrating KAR-currents evoked by glutamate uncaging on TEs of CA3 PCs in organotypic slice cultures prepared from GluK2^{+/+} and GluK2^{-/-} mice, not transfected (NT) or transfected with 3 ng μl⁻¹ of wt or mutated GluK2a cDNA (Δ14 and Δ29). (e) Bar graphs summarizing KAR/AMPA ratios obtained from the experiments presented in d. GluK2^{+/+} NT: n = 11 cells; GluK2^{-/-} NT: n = 11; GluK2^{-/-} + GluK2a: n = 9 cells; GluK2Δ14: n = 11 cells; GluK2Δ29: n = 15 cells; 24 mice. In all panels, values are presented as mean ± s.e.m. of n experiments. Data were compared using one-way analysis of variance followed by Dunnett’s multiple comparison test (NS, not significant; P > 0.05, **P < 0.01 and ***P < 0.001).

to mf-CA3 synapses. Interestingly, re-expression of both GluK2aΔ14 and GluK2aΔ29 strongly reduced KAR-EPSCs (KAR/AMPA ratio, GluK2aΔ14: 4.8 ± 0.8%; P < 0.01; GluK2aΔ29: 3.4 ± 0.7%; P < 0.001), albeit trafficking of GluK2aΔ14 and GluK2aΔ29 to the plasma membrane is not impaired in dissociated cultured neurons³⁸. In addition, the biophysical properties of GluK2a truncated up to the last 29 amino acids do not differ from full-length GluK2a³⁹. Hence, the decreased amplitude of KAR-EPSCs may be explained by impaired recruitment or stabilization of mutated KARs at mf-CA3 synapses. Further truncation of the last 39 amino acids (GluK2aΔ39) is known to decrease surface trafficking of GluK2a due to defect in forward trafficking of KARs to the plasma membrane^{38,39}. Accordingly, expression of GluK2aΔ39 (3 ng μl⁻¹) in GluK2^{-/-} mice led to KARs-EPSCs with largely reduced relative amplitude with respect to WT (KAR/AMPA ratio, WT: 10.0 ± 1.3; GluK2aΔ39: 2.0 ± 0.5; P < 0.001). KAR currents evoked by glutamate uncaging on TEs following re-expression of GluK2aΔ14 (3 ng μl⁻¹) and GluK2aΔ29 displayed largely decreased mean amplitudes as compared with WT (mean amplitude, WT: 59.7 ± 12.0 pA; GluK2aΔ14: 15.9 ± 1.8 pA; GluK2aΔ29: 19.3 ± 2.6 pA; P < 0.001; Fig. 6d,e). No detectable extrasynaptic KAR currents were however observed in the soma following re-expression of GluK2aΔ14 or GluK2aΔ29 in GluK2^{-/-} mice (Supplementary

Fig. 4). Together, these results confirm that the 14 last aminoacids of GluK2a CTD are important for the stabilization of KARs at mf-CA3 synapses.

N-cadherin is involved in synaptic stabilization KARs. GluK2a interacts with N-cadherin/β-catenin complexes through its CTD domain; this interaction involves the 14 last amino acids of the CTD and is necessary for N-cadherin-mediated recruitment and aggregation of membrane KARs in heterologous cells¹⁶. As truncation of this 14 amino-acid sequence strongly decreased KAR-EPSC amplitude, we tested the role of the N-cadherin/β-catenin complex in the stabilization of KARs at mf-CA3 synapses. For this, we first used a dominant-negative approach in organotypic cultures by overexpressing in CA3 cells an N-cadherin protein lacking the entire extracellular domain necessary for homophilic adhesions and transsynaptic adhesion (Ncad-ΔE)⁴⁰. This mutant acts as a dominant-negative construct by sequestering α- and β-catenins⁴¹, thereby interfering with the binding of GluK2a to endogenous N-cadherin. Under these conditions, we observed a strong reduction in the amplitude of KAR-EPSCs, as quantified by the KAR/AMPA ratio (mean KAR/AMPA ratio, GFP: 17.3 ± 3.9%; Ncad-ΔE: 5.8 ± 1.1%; P < 0.05; Fig. 7a,b). As a control, the net amplitude of AMPAR-EPSCs was not affected by the overexpression of

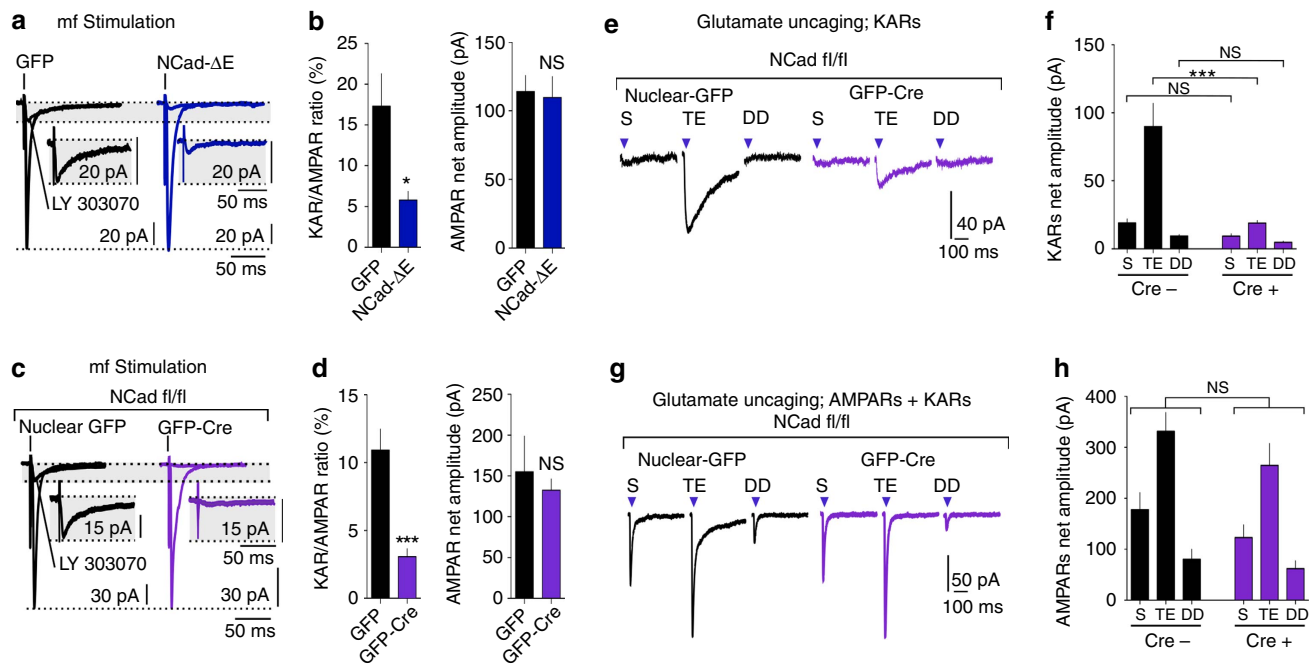


Figure 7 | N-cadherin is necessary for the stabilization of synaptic KARs. (a,b) Averaged synaptic currents evoked by mf stimulation (3Hz) in WT CA3 PCs from organotypic slices transfected with GFP or NCad-ΔE ($30 \text{ ng } \mu\text{l}^{-1}$) in the absence and in the presence of $25 \text{ } \mu\text{M}$ LY303070, to isolate the AMPAR and the KAR component, respectively. Insert enlargements of isolated KAR-EPSCs. Graphs summarizing KAR/AMPAR ratios and net amplitude of AMPAR-EPSCs obtained from experiments presented in a. GFP: $n = 6$ cells; NCad-ΔE: $n = 6$ cells; 7 mice. (c,d) Averaged synaptic currents evoked by mf stimulation (3Hz) in CA3 PCs from NCad^{fl/fl} organotypic slices transfected with nuclear GFP or GFP-Cre ($20 \text{ ng } \mu\text{l}^{-1}$), in the absence and in the presence of $25 \text{ } \mu\text{M}$ LY303070, to isolate AMPAR and KAR-EPSCs, respectively. Insert, enlargements of isolated KAR-EPSCs. Graphs summarizing KAR/AMPAR ratios and net amplitudes of AMPAR-EPSCs obtained from experiments in c. Nuclear-GFP: $n = 7$ cells; GFP-Cre: $n = 6$ cells; 8 mice. (e,f) Sample traces illustrating KAR currents evoked by glutamate uncaging ($25 \text{ } \mu\text{M}$ LY303070) in different compartments (S, TE and DD) of CA3 PCs from NCad^{fl/fl} organotypic slices electroporated either with nuclear-GFP or GFP-Cre. Graph summarizing average net amplitude of evoked KAR currents. Nuclear-GFP; uncaging sites: S, $n = 11$; TE, $n = 11$; DD, $n = 10$. Experiments performed on 11 cells, 6 slices and 4 mice. GFP-Cre; uncaging sites: S, $n = 8$; TE, $n = 8$; DD, $n = 8$. Experiments performed on eight cells, four slices and four mice. (g,h) Sample traces illustrating AMPAR-KAR currents evoked by glutamate uncaging in different compartments of CA3 PCs (S, TE and DD) from NCad^{fl/fl} organotypic slices electroporated with either nuclear-GFP or GFP-Cre (S, TE and DD). Graph summarizing average net amplitude of evoked AMPAR-KAR currents. Nuclear-GFP; uncaging sites: S, $n = 9$; TE, $n = 9$; DD, $n = 8$. Experiments performed on nine cells, four slices and four mice. GFP-Cre; uncaging sites: S, $n = 8$; TE, $n = 8$; DD, $n = 8$. Experiments performed on eight cells, four slices and four mice. All experiments include bicuculline ($10 \text{ } \mu\text{M}$), D-AP5 ($50 \text{ } \mu\text{M}$) and NBQX (150 nM). In all panels, values are presented as mean \pm s.e.m. of n experiments. Data were compared using unpaired t -test (NS, not significant; $P > 0.05$, $*P < 0.05$ and $***P < 0.001$).

NCad-ΔE (mean net amplitude, GFP: $114.1 \pm 11.5 \text{ pA}$; NCad-ΔE: $109.8 \pm 15.2 \text{ pA}$; Fig. 7b).

NCad-ΔE may potentially affect signalling through different types of cadherins, for example, cadherin-9, which is also present at mf-CA3 synapses⁴². To show a specific link between KARs and N-cadherin, we deleted endogenous N-cadherin by expression of the Cre recombinase in CA3 PCs from N-cadherin floxed mice (N-Cadherin^{fl/fl})⁴³ with a plasmid coding for GFP-cre or for nuclear GFP as a control (Fig. 7c,d). We also observed a marked reduction of KAR-EPSCs in CA3 PCs on knockdown of N-cadherin (10–12 days after electroporation) as quantified by the KAR/AMPAR ratio (mean KAR/AMPAR ratio, nuclear GFP: $10.9 \pm 1.6\%$; GFP-cre: $3.1 \pm 0.6\%$; $P < 0.0001$; Fig. 7c,d). The net amplitude of AMPAR-EPSCs at mf-CA3 synapses was not affected by downregulation of N-cadherin (mean net amplitude, nuclear GFP: $155.2 \pm 43.7 \text{ pA}$; GFP-cre: $132.5 \pm 13.8 \text{ pA}$; Fig. 7d). Similarly, the amplitude and frequency of AMPAR-mediated mEPSCs were not different in CA3 PCs electroporated with either GFP-cre or nuclear GFP (Supplementary Fig. 5). Finally, knockdown of N-cadherin led to a significant decrease in the amplitude of KAR currents mediated by focal glutamate uncaging onto TEs (mean amplitude, nuclear GFP: soma, $19.1 \pm 2.9 \text{ pA}$; TE, $89.9 \pm 17.1 \text{ pA}$; DD, $9.5 \pm 1.0 \text{ pA}$; GFP-cre: soma, $9.4 \pm 1.6 \text{ pA}$; TE,

$18.9 \pm 1.7 \text{ pA}$; DD, $4.7 \pm 0.8 \text{ pA}$; Fig. 7e,f). In contrast, the amplitude of AMPAR-mediated currents were not significantly reduced on N-cadherin knockdown with respect to control conditions (mean amplitude, nuclear GFP: soma, $177.5 \pm 33.3 \text{ pA}$; TE, $331.2 \pm 36.6 \text{ pA}$; DD, $80.2 \pm 19.8 \text{ pA}$; GFP-cre: soma, $122.9 \pm 24.8 \text{ pA}$; TE, $264.6 \pm 42.7 \text{ pA}$; DD, $61.9 \pm 15.4 \text{ pA}$; Fig. 7g,h). We obtained similar results when the knockdown of N-cadherin was induced *in vivo* by stereotaxic infection of N-Cadherin^{fl/fl} mice with a virus (AAV 2.9) coding for GFP-Cre, under the control of a synapsin promoter in the CA3 area of the hippocampus. Acute brain slices were prepared and patch-clamp recordings of CA3 PCs were performed 3–4 weeks after infection (Supplementary Fig. 5). Altogether, these results indicate that the N-cadherin/ β -catenin complex is involved in the recruitment and/or stabilization of KARs at mf-CA3 synapses.

Discussion

We show that the strict compartmentalization of KARs at mf-CA3 synapses in CA3 PCs is readily preserved in organotypic slices, providing a much improved model over dissociated cultured neurons, which express functional native KARs, however not synaptically. Similar to that in acute slices, focal glutamate

uncaging in CA3 PCs from WT organotypic slices reveals a highly segregated subcellular distribution of functional KARs. KAR currents can only be activated when the uncaging spot is focalized on TEs, but not on the soma, on the proximal dendritic shaft or on distal dendrites and spines. Pathway-specific localization of postsynaptic KARs may be a general feature, which has indeed been reported in pyramidal neurons of the medial entorhinal cortex⁴⁴ and at climbing fibre synapses onto Purkinje cells⁴⁵, also indicating that confined expression of KARs can be observed in the absence of a morphologically specialized postsynaptic element such as TEs. The spatial resolution of our technique, together with the spacing between PSDs of mf-CA3 synapses (*ca.* 500 nm)^{28,46}, does not allow to exclude the presence of KARs at perisynaptic sites between the various PSDs on TEs. However, functional studies using blockers of glutamate transporters to probe for activation of KARs by glutamate spillover do not favour the presence of KARs at perisynaptic sites^{10,47}. Nonetheless, our experiments reveal a striking difference between the two related iGluR families AMPARs and KARs. Whereas AMPARs are present at both synaptic and extrasynaptic (soma and dendritic shafts) sites in acute and organotypic slices, KARs are exclusively distributed at a particular synaptic input and absent from extrasynaptic sites. Extrasynaptic AMPARs may serve as a pool of receptors ready to be used for LTP of AMPAR-EPSCs relying on surface diffusion⁴⁸. The lack of a pool of extrasynaptic KARs may explain the inability to induce LTP of KAR-EPSCs⁹, except in artificial conditions where AMPARs are absent⁴⁹.

With this model system in hands, we identified molecular sequences of the major KAR subunit GluK2 required for the strict subcellular segregation observed. We transfected CA3 PCs from GluK2^{-/-} slices to re-express the GluK2a subunit and mutants thereof, based on the fact that GluK2 is an essential component of KARs in CA3 PCs¹¹. From a methodological standpoint, we found that transfection of a precise amount of GluK2a cDNA, using single-cell electroporation, was necessary for a faithful restoration of the strict subcellular segregation of KARs. With concentrations of cDNA above 10 ng μl⁻¹, re-expression of GluK2a led to the abnormal expression of KARs throughout the somatodendritic compartment of CA3 PCs. Beside the strong methodological warning about the importance of using a semi-quantitative replacement strategy, these results also suggest that the stringent subcellular segregation of native KARs—the exclusion from extrasynaptic sites—depends at least in part on the amount of the GluK2 subunit expressed by CA3 PCs. Hence, in physiological conditions, one can speculate that the amount of GluK2-containing KARs is strongly controlled, either at the transcriptional or postranscriptional level. Not much is known about transcriptional regulation of KARs. At the posttranscriptional level, SUMOylation of GluK2a leads to the removal of KARs from the postsynaptic membrane, leading to a decrease in KAR-mediated synaptic transmission⁵⁰. In addition, the presence of GluK2 in the plasma membrane can be controlled by its interaction with Parkin, which interacts and ubiquitinates GluK2, and as a consequence regulates GluK2 levels and KAR currents in cultured neurons⁵¹. It would thus be interesting to map KARs in CA3 PCs in the absence of Parkin, or in conditions of reduced SUMOylation of GluK2. The large ectopic KAR currents evoked by brief ultraviolet uncaging flashes observed in CA3 PCs transfected with high concentrations of cDNA displayed fast decay kinetics, which are reminiscent of recombinant homomeric GluK2 KARs³¹ and are very different from native KARs recorded on TEs. The block of ectopic KAR currents by UBP310, an antagonist of heteromeric GluK2/GluK5 receptors but not of homomeric GluK2 (ref. 33), indicates that ectopic KARs are probably homo-tetramers. This suggests that the availability of GluK4 or GluK5 to form heteromers are in controlled and limited

amounts in CA3 PCs. Hence, non-controlled overexpression of GluK2 leads to the loss of the strict compartmentalization of KARs in CA3 PCs giving rise to abnormal homomeric GluK2 at extrasynaptic sites.

Re-expression of GluK2a in CA3 PCs of GluK2^{-/-} mice restores expression of KARs at mf-CA3 synapses. Interestingly, the amplitude and kinetics of KAR-EPSCs appear independent of the amount of cDNA transfected, a finding compatible with a synaptic slot hypothesis⁴⁸. Whatever the cDNA concentration, KAR-EPSCs cannot be recorded at A/C synapses. We thus propose that only a limited amount of slots selective for KARs are available at mf-CA3 synapses. Once these slots are occupied, overexpressed KARs invade extrasynaptic sites. The limited slots for KARs correlates with the observation that in physiological conditions, KAR-EPSCs can undergo LTD^{26,52,53}, but not LTP. LTD may correspond to the diffusion of heteromers of GluK2 and/or GluK4 and GluK5 out of synapses, followed by rapid internalization. GluK4 and GluK5 are certainly essential elements in controlling the synaptic amount of KARs^{26,52} and removing both GluK4 and GluK5 abolishes KAR-EPSCs³².

What constitutes a KAR synaptic slot remains an open question. Possibilities include PDZ-domain-containing proteins such as PSD95, PICK or GRIP^{14,15,37,54}, although re-expression of a mutated GluK2a subunit lacking the four last amino acids responsible for the interaction with PDZ domain proteins did not affect KAR-EPSCs. In contrast, removal of the last 14 amino acids of GluK2a strongly had an impact on the amplitude of KAR-EPSCs. Interestingly, these last 14 amino acids are essential for the interaction of GluK2-containing KARs with N-cadherin/β-catenin complexes, albeit this interaction is likely to be indirect¹⁶ and other proteins could potentially interact with GluK2 through these amino acids. N-cadherins are synaptic adhesion proteins implicated in synapse formation and maturation⁵⁵. Activation of N-cadherins by ligand-covered latex beads recruits GluK2a to N-cadherin/β-catenin complexes in heterologous cells in a manner, which strictly depends on the last 14 aa of GluK2a¹⁵. Here we demonstrate that overexpression of a dominant-negative N-cadherin or knocking down N-cadherin in slice cultures or *in vivo* strongly reduces KAR-EPSCs at mf-CA3 synapses without impacting on basal synaptic properties. This decrease in KAR-EPSCs was not accompanied with a detectable increase in extrasynaptic KARs, suggesting that unstabilized synaptic KARs may undergo rapid endocytosis. Although N-cadherin binds AMPARs through an interaction with the N-terminal extracellular domain of GluA2 (ref. 56), or intracellularly⁵⁷, AMPARs were surprisingly not affected by the removal of N-cadherin in our experimental conditions. This was indicated by the lack of effect of N-cadherin inactivation on the amplitude of evoked AMPAR-EPSCs, mEPSCs and AMPAR currents induced by focal glutamate uncaging. Possibly, AMPARs may be stabilized at the PSD in mature synapses via additional transsynaptic adhesion molecules, such as neuroligins or leucine-rich repeat transmembrane (LRRTM) proteins. Hence, our data indicate that N-cadherins specifically recruit and/or stabilize KARs at mf-CA3 synapses.

Synaptic specificity is probably mediated by a network of synaptic molecules. N-cadherins appear to be one of the partner molecules responsible for the synaptic stabilization of KARs at mf-CA3 synapses. Accordingly, it is interesting to note that N-cadherin labelling is particularly intense in the dendritic shaft of CA3 PCs in the stratum lucidum⁵⁸. Other partners are likely to play a role in the subcellular segregation of KARs at these particular synaptic sites. Synaptic specificity in the brain involves differential expression of type II cadherin genes⁵⁵, such as Cadherin-9, which is expressed in both the DG and CA3 PCs, and appears essential for the specific formation of mf-CA3 synapses

during development⁴². Cadherin-9 may also play a role in specifying the functional properties of mature mf-CA3 synapses, although this has yet to be explored. An association between N-cadherin and Cadherin-9, possibly assembled as heterodimers, could be essential for the maintenance of specific synaptic features. One can speculate that the loss of Cadherin-9 could similarly impact KAR-EPSCs. Interestingly, a recent report identifies a role for the C1q-like proteins C1ql2 and C1ql3 in the recruitment of KARs at mf-CA3 synapses by direct interaction with the extracellular domain of GluK2 and/or GluK4 subunits. One can speculate that the C1ql2/3 proteins secreted by mfs may regulate the recruitment of KARs and provide input specificity, whereas N-cadherins would stabilize synaptic KARs through indirect interactions with the cytoplasmic domain of GluK2a.

Understanding the molecular mechanisms underlying the synaptic recruitment of KARs at mf-CA3 synapses could also shed light on the pathological process through which aberrant KARs are recruited at recurrent mf onto DG cells in temporal lobe epilepsy⁵⁹. Neutralization of these aberrant KARs markedly attenuates epileptic seizures in a mouse model of temporal lobe epilepsy⁶⁰. The molecular mechanisms underlying synaptic segregation of KARs probably bear similarities at both mf-CA3 synapses and recurrent mf synapses onto DG cells⁶¹.

In conclusion, multiple mechanisms combine to control the specific subcellular localization of KARs at mf-CA3 synapses, including a stringent control of the amount of GluK2 subunit in CA3 PCs, a limited number of postsynaptic slots for KARs and the recruitment/stabilization of KARs by transsynaptic mechanisms which may involve a coordination between secreted C1ql2/3 proteins, cadherin-9 and N-cadherin.

Methods

DNA constructs. GluK2a WT and GluK2a C-terminal mutant cDNAs used in the present study were described previously and were expressed under the control of a cytomegalovirus (CMV) promoter^{15,38}. DNA plasmids were dissolved at various concentrations in the electroporation solution: GluK2 WT, GluK2 C-terminal mutant and SEP-GluK2 (ref. 62) cDNAs at concentration between 3 and 80 ng μl^{-1} ; GFP at 30 ng μl^{-1} (CMV); tdTomato, 20 ng μl^{-1} (CMV); NCad- ΔE^{63} at 30 ng μl^{-1} (CMV); GFP-cre at 30 ng μl^{-1} (CMV) and nuclear GFP 30 ng μl^{-1} (CMV). In all uncaging experiments, CA3 PCs were co transfected with GFP or tdTomato to visualize cell morphology. In uncaging experiments, NT refers to cells not transfected with GluK2a (or NCad- ΔE , GFP-cre or nuclear GFP) plasmids, but expressing only GFP or tdTomato. In experiments presented in Figs 4 and 5 and Supplementary Fig. 5e–g, NT refers to CA3 PCs not transfected with any constructs.

Slice culture preparation and transfection. Organotypic hippocampal slice (300 μm thickness) cultures were prepared from P5 to P7 GluK2^{-/-} and WT FVB mice as described previously²⁶, and according to the guidelines of the University of Bordeaux/CNRS Animal Care and Use Committee. Three to 4 days after plating, the medium was replaced and then changed every 2–3 days. After 7 days *in vitro*, visually identified CA3 PCs were transfected by single-cell electroporation. For this, slices were placed in the microscope chamber in the presence of a small volume of a sterile pre-warmed (37 °C) HEPES-based artificial cerebrospinal fluid (ACSF) composed of 145 mM NaCl, 2.5 mM KCl, 2 mM CaCl_2 , 1 mM MgCl_2 , 10 mM HEPES and 10 mM glucose, adjusted to 310 mOsm l^{-1} and pH 7.4 with NaOH at room temperature. Electroporation pipettes (8–10 m Ω) were filled with a solution containing the following: 140 mM CH_3KSO_3 , 2 mM MgCl_2 , 4 mM NaCl, 5 mM P-creatine, 3 mM Na_2ATP , 0.33 mM GTP, 0.2 mM EGTA and 10 mM HEPES adjust to 300 mOsm l^{-1} and pH 7.2 with KOH. cDNA was added to the internal solution the day of the experiment. The electroporation pipette was approached to the cell body in loose cell-attached configuration. A train of stimulation to the cell body (50 square pulses, 600 μs duration, at 100 Hz with an amplitude of -11.5 V). The pulses were delivered by a stimulating unit controlled by an EPC9 amplifier (HEKA Elektronik, Lambrecht/Pfalz, Germany) and the pipette was slowly retracted and positioned on an other cell body.

In vivo virus injection and acute slices preparation. Stereotaxic viral injections were performed on 3-week-old male C57bl6 N-Cadherin^{fl/fl} mice. The mice were injected with 300 nl (55 nl min^{-1}) of an AAV2/9 encoding for GFP-Cre under a synapsin promoter (AAV2/9.hsynapsin.hghintron.GFP.cre.wpre.sv40; titer 1.33¹¹) in the CA3 area of the right hippocampus with the following coordinates:

+1.90 mm mediolateral (ML), -1.90 mm anteroposterior (AP) and -1.9 mm dorsoventral (DV). For acute slices recordings, transverse hippocampal slices (320 μm thick) were obtained from 17- to 19-day-old FVB GluK2^{-/-} and GluK2^{+/+} mice and from 2-month-old N-Cadherin^{fl/fl} mice anaesthetized with ketamine (75 mg kg^{-1}) and xylazine (10 mg kg^{-1}) mix, and killed by decapitation.

Electrophysiology. Whole-cell patch-clamp experiments were performed at 33 °C from CA3 PCs expressing or not GFP 3–4 days after transfection. Whole-cell voltage-clamp recordings were performed with 3–4 M Ω electrodes filled with a solution containing 140 mM CsCH_3SO_3 , 2 mM MgCl_2 , 4 mM NaCl, 5 mM P-creatine, 3 mM Na_2ATP , 0.33 mM GTP, 0.2 mM EGTA and 10 mM HEPES adjust to 300 mOsm l^{-1} and pH 7.2 with CsOH. In experiments in which mf or A/C inputs were electrically stimulated by an extracellular electrode, slices were perfused with an extracellular solution (ACSF) composed of: 125 mM NaCl, 2.5 mM KCl, 1.25 mM NaH_2PO_4 , 26 mM NaHCO_3 , 2.3 mM CaCl_2 , 1.3 mM MgCl_2 and 25 mM glucose saturated with 95% O_2 /5% CO_2 . Mf synaptic responses were evoked by minimal stimulation⁶⁴ by placing a patch pipette filled with aCSF in the hilus of the DG. A/C excitatory stimulations were evoked by placing the pipette in the stratum radiatum above the CA3 PC layer. The distinct nature of the stimulated inputs was confirmed by recording short-term plasticity properties. These experiments were performed at 30–32 °C in the presence of pharmacological drugs in the aCSF: NBQX 150 nM, DAP-5 50 μM and bicuculline 10 μM . For experiments with synaptic stimulation, one cell was recorded per slice. KAR currents were pharmacologically isolated in the presence of LY 303070 25 μM , a selective AMPAR antagonist. For glutamate uncaging experiments, slices were bathed with 2 ml of HEPES-based ACSF (room temperature) composed of 140 mM NaCl, 3.5 mM KCl, 6 mM HEPES, 4 mM Na-HEPES, 2.3 mM CaCl_2 , 1.3 mM MgCl_2 , 10 mM glucose and 1 mM sodium pyruvate. One to three cells were recorded per slice. Glutamate receptors were activated by glutamate uncaging in the presence of MNI glutamate 500 μM (2 ms duration at 0.1 Hz). Glutamate uncaging was performed on a Nikon FN1 microscope equipped with a $\times 60$ lens (numerical aperture 1.00) and a 405 nm Obis laser (Coherent, Germany; 50 mW CW) controlled by a Digitimer DS2A (Digitimer, Welwyn, UK).

The access resistance was $<20\text{ M}\Omega$ and cells were discarded if it changed by $>20\%$. No series resistance compensation was used. Recordings were made using EPC 9 or EPC10 amplifiers (HEKA Elektronik, Lambrecht/Pfalz, Germany), were filtered at 0.5–1 kHz, digitalized at 5 kHz and stored on a personal computer for further analysis (IGOR PRO 6.2; WaveMetrics, Lake Oswego, OR). Values are presented as mean \pm s.e.m. Electrophysiological analysis was performed with the IGOR PRO software through NeuroMatic v2.6 plugin. The decaying phase of the currents was fitted with a function of the following form: $y(t) = \sum A_i \exp(-t/\tau_i)$, where A_i is the fraction of respective components ($\sum A_i = 1$) and τ_i is the time constant τ_{fit} calculated using the formula $\tau_{\text{fit}} = \sum A_i \tau_i$. A maximum of two exponential components was used. It has been shown that in organotypic slice cultures A/C fast synaptic transmission, unlike mf-CA3, can be in part mediated by P2X receptors activated by ATP^{3,65}. We have observed similar residual currents in our preparation both in the presence of NBQX 25 μM and in GluK2^{-/-} animals (data not shown). For this reason, to quantify KAR-mediated EPSCs at A/C input we have subtracted the residual current after application of LY 30,3070, with the residual current after the further application of NBQX (to block AMPARs and KARs).

Immunohistochemistry and SEP-GluK2a. Live organotypic hippocampal slices in which CA3-PCs were electroporated with TdTomato and SEP-GluK2a were labelled with 200 nM GFP-nanobody coupled to ATTO647N (ATTO-TEC)³⁶ in a dark chamber for 30–60 min at room temperature in the same ACSF used for uncaging experiments supplemented with 1% globulin-free BSA (Sigma, St Louis, MO). Slices were then rinsed and fixed in 4% paraformaldehyde (PFA) containing 20% sucrose for 2 h at 4 °C, before rinsing with PBS and mounting in mowiol 4–88 (Sigma). Confocal images were acquired sequentially on a commercial Leica TCS SPE microscope equipped with three laser diodes (488, 561, 647 nm) using a $\times 63$ oil objective and a pinhole opened to one time the Airy disk. The number of SEP-GluK2 clusters per micrometre was determined using Metamorph software (Molecular Devices, USA). Briefly, z-projections of the stacks in the 488 (SEP) and 635 (ATTO647N) channels were segmented after background subtraction. Segmented images were overlaid and GluK2 clusters were defined as individual spots that were present in both channels and co-localized within determined areas of the neuron (soma, TEs and DDs).

In Fig. 1 and Supplementary Fig. 1, the confocal images were obtained after fixation of organotypic slices following glutamate uncaging on organotypic slices from WT FVB mice electroporated with a cDNA construct coding for GFP-N1. The slices were fixed with PFA, 30% sucrose for 15 min at room temperature. After blocking within PBS, 10% fetal calf serum for 1 h, we immunodetected GFP by incubating the slices with a mouse monoclonal antibody anti-GFP (Roche; dilution 1/200, overnight at 4 °C) in PBS containing 0.2% Triton and 5% SVF. After washing three times in PBS, the slices were incubated with a fluorophore-coupled secondary antibody anti-mouse (Life Technologies) in PBS containing 5% SVF and 0.2% Triton (dilution 1:1,000, for 2 h at room temperature). Finally, the slices were washed three times at room temperature with PBS and coverslipped in Vectashield medium (Vector).

Confocal laser-scanning fluorescence microscopy and image analysis.

Confocal image stacks of PFA-fixed organotypic slices were acquired with a Leica DM6000 TCQS SP8 X white laser-scanning microscope using the objective Leica HCX PL Apo CS $\times 100$ oil numerical aperture 1.4. Images were processed with ImageJ 1.49d software (Wayne Rasband, National Institutes of Health, USA). Illustrations correspond to two-dimensional maximal projections of three-dimensional acquired confocal stacks smoothed by the median filter.

Drugs. All drugs were obtained from Tocris Cookson (Bristol, UK), Sigma or Ascent Scientific (Bristol, UK).

Data availability. The data that support the findings of this study are available from the corresponding author on request.

References

- Williams, M. E., de Wit, J. & Ghosh, A. Molecular mechanisms of synaptic specificity in developing neural circuits. *Neuron* **68**, 9–18 (2010).
- Henze, D. A., Urban, N. N. & Barrionuevo, G. The multifarious hippocampal mossy fiber pathway: a review. *Neuroscience* **98**, 407–427 (2000).
- Nicoll, R. A. & Schmitz, D. Synaptic plasticity at hippocampal mossy fibre synapses. *Nat. Rev. Neurosci.* **6**, 863–876 (2005).
- Paoletti, P., Bellone, C. & Zhou, Q. NMDA receptor subunit diversity: impact on receptor properties, synaptic plasticity and disease. *Nat. Rev. Neurosci.* **14**, 383–400 (2013).
- Bettler, B. & Mulle, C. Review: neurotransmitter receptors. II. AMPA and kainate receptors. *Neuropharmacology* **34**, 123–139 (1995).
- Contractor, A., Mulle, C. & Swanson, G. T. Kainate receptors coming of age: milestones of two decades of research. *Trends Neurosci.* **34**, 154–163 (2011).
- Lerma, J. & Marques, J. M. Kainate receptors in health and disease. *Neuron* **80**, 292–311 (2013).
- Rodríguez-Moreno, A. & Sihra, T. S. Kainate receptors with a metabotropic modus operandi. *Trends Neurosci.* **30**, 630–637 (2007).
- Carta, M., Fièvre, S., Gorlewicz, A. & Mulle, C. Kainate receptors in the hippocampus. *Eur. J. Neurosci.* **39**, 1835–1844 (2014).
- Castillo, P. E., Malenka, R. C. & Nicoll, R. A. Kainate receptors mediate a slow postsynaptic current in hippocampal CA3 neurons. *Nature* **388**, 182–186 (1997).
- Mulle, C. *et al.* Altered synaptic physiology and reduced susceptibility to kainate-induced seizures in GluR6-deficient mice. *Nature* **392**, 601–605 (1998).
- Ruiz, A., Sachidhanandam, S., Urvik, J. K., Coussen, F. & Mulle, C. Distinct subunits in heteromeric kainate receptors mediate ionotropic and metabotropic function at hippocampal mossy fiber synapses. *J. Neurosci.* **25**, 11710–11718 (2005).
- Darstein, M., Petralia, R. S., Swanson, G. T., Wenthold, R. J. & Heinemann, S. F. Distribution of kainate receptor subunits at hippocampal mossy fiber synapses. *J. Neurosci.* **23**, 8013–8019 (2003).
- Garcia, E. P. *et al.* SAP90 binds and clusters kainate receptors causing incomplete desensitization. *Neuron* **21**, 727–739 (1998).
- Coussen, F. *et al.* Co-assembly of two GluR6 kainate receptor splice variants within a functional protein complex. *Neuron* **47**, 555–566 (2005).
- Coussen, F. *et al.* Recruitment of the kainate receptor subunit glutamate receptor 6 by cadherin/catenin complexes. *J. Neurosci.* **22**, 6426–6436 (2002).
- Copits, B. A. & Swanson, G. T. Kainate receptor post-translational modifications differentially regulate association with 4.1N to control activity-dependent receptor endocytosis. *J. Biol. Chem.* **288**, 8952–8965 (2013).
- Zhang, W. *et al.* A transmembrane accessory subunit that modulates kainate-type glutamate receptors. *Neuron* **61**, 385–396 (2009).
- Copits, B. A., Robbins, J. S., Frausto, S. & Swanson, G. T. Synaptic targeting and functional modulation of GluK1 kainate receptors by the auxiliary neuropilin and Tolloid-like (NETO) proteins. *J. Neurosci.* **31**, 7334–7340 (2011).
- Straub, C. *et al.* Distinct functions of kainate receptors in the brain are determined by the auxiliary subunit Neto1. *Nat. Neurosci.* **14**, 866–873 (2011).
- Fisher, J. L. & Mott, D. D. The auxiliary subunits Neto1 and Neto2 reduce voltage-dependent inhibition of recombinant kainate receptors. *J. Neurosci.* **32**, 12928–12933 (2012).
- Tang, M. *et al.* Neto1 is an auxiliary subunit of native synaptic kainate receptors. *J. Neurosci.* **31**, 10009–10018 (2011).
- Copits, B. A. & Swanson, G. T. Dancing partners at the synapse: auxiliary subunits that shape kainate receptor function. *Nat. Rev. Neurosci.* **13**, 675–686 (2012).
- Palacios-Filardo, J., Aller, M. I. & Lerma, J. Synaptic targeting of kainate receptors. *Cerebral Cortex* **26**, 1464–1472 (2014).
- Benson, D. L. & Huntley, G. W. Synapse adhesion: a dynamic equilibrium conferring stability and flexibility. *Curr. Opin. Neurobiol.* **22**, 397–404 (2012).
- Carta, M. *et al.* CaMKII-dependent phosphorylation of GluK5 mediates plasticity of kainate receptors. *EMBO J.* **32**, 496–510 (2013).
- Trigo, F. F., Corrie, J. E. T. & Ogden, D. Laser photolysis of caged compounds at 405nm: Photochemical advantages, localisation, phototoxicity and methods for calibration. *J. Neurosci. Methods* **180**, 9–21 (2009).
- Rollenhagen, A. *et al.* Structural determinants of transmission at large hippocampal mossy fiber synapses. *J. Neurosci.* **27**, 10434–10444 (2007).
- Wilke, S. A. *et al.* Specific disruption of hippocampal mossy fiber synapses in a mouse model of familial Alzheimer's disease. *PLoS ONE* **9**, e84349 (2014).
- Contractor, A. *et al.* Loss of kainate receptor-mediated heterosynaptic facilitation of mossy-fiber synapses in KA2-/- mice. *J. Neurosci.* **23**, 422–429 (2003).
- Barberis, A., Sachidhanandam, S. & Mulle, C. GluR6/KA2 kainate receptors mediate slow-deactivating currents. *J. Neurosci.* **28**, 6402–6406 (2008).
- Fernandes, H. B. *et al.* High-affinity kainate receptor subunits are necessary for ionotropic but not metabotropic signaling. *Neuron* **63**, 818–829 (2009).
- Pinheiro, P. S. *et al.* Selective block of postsynaptic kainate receptors reveals their function at hippocampal mossy fiber synapses. *Cereb. Cortex* **23**, 323–331 (2013).
- González-González, I. M. & Henley, J. M. Postsynaptic kainate receptor recycling and surface expression are regulated by metabotropic autoreceptor signalling. *Traffic* **14**, 810–822 (2013).
- Ries, J., Kaplan, C., Platonova, E., Eghlidi, H. & Ewers, H. A simple, versatile method for GFP-based super-resolution microscopy via nanobodies. *Nat. Methods* **9**, 582–584 (2012).
- Chamma, I. *et al.* Mapping the dynamics and nanoscale organization of synaptic adhesion proteins using monomeric streptavidin. *Nat. Commun.* **7**, 10773 (2016).
- Hirbec, H. *et al.* Rapid and differential regulation of AMPA and kainate receptors at hippocampal mossy fibre synapses by PICK1 and GRIP. *Neuron* **37**, 625–638 (2003).
- Jaskolski, F. *et al.* Subunit composition and alternative splicing regulate membrane delivery of kainate receptors. *J. Neurosci.* **24**, 2506–2515 (2004).
- Yan, S. *et al.* A C-terminal determinant of GluR6 kainate receptor trafficking. *J. Neurosci.* **24**, 679–691 (2004).
- Chazeau, A. *et al.* Mechanical coupling between transsynaptic N-cadherin adhesions and actin flow stabilizes dendritic spines. *Mol. Biol. Cell* **26**, 859–873 (2015).
- Riehl, R. *et al.* Cadherin function is required for axon outgrowth in retinal ganglion cells *in vivo*. *Neuron* **17**, 837–848 (1996).
- Williams, M. E. *et al.* Cadherin-9 regulates synapse-specific differentiation in the developing hippocampus. *Neuron* **71**, 640–655 (2011).
- Li, J. *et al.* Cardiac-specific loss of N-cadherin leads to alteration in connexins with conduction slowing and arrhythmogenesis. *Circ. Res.* **97**, 474–481 (2005).
- Beed, P. S., Salmen, B. & Schmitz, D. GluK2-mediated excitability within the superficial layers of the entorhinal cortex. *PLoS ONE* **4**, e5576 (2009).
- Huang, Y. H., Dykes-Hoberg, M., Tanaka, K., Rothstein, J. D. & Bergles, D. E. Climbing fiber activation of EAAT4 transporters and kainate receptors in cerebellar Purkinje cells. *J. Neurosci.* **24**, 103–111 (2004).
- Wilke, S. A. *et al.* Deconstructing complexity: serial block-face electron microscopic analysis of the hippocampal mossy fiber synapse. *J. Neurosci.* **33**, 507–522 (2013).
- Bureau, I., Dieudonne, S., Coussen, F. & Mulle, C. Kainate receptor-mediated synaptic currents in cerebellar Golgi cells are not shaped by diffusion of glutamate. *Proc. Natl Acad. Sci. USA* **97**, 6838–6843 (2000).
- Choquet, D. & Triller, A. Perspective. *Neuron* **80**, 691–703 (2013).
- Granger, A. J., Shi, Y., Lu, W., Cerpas, M. & Nicoll, R. A. LTP requires a reserve pool of glutamate receptors independent of subunit type. *Nature* **493**, 495–500 (2013).
- Martin, S., Nishimune, A., Mellor, J. R. & Henley, J. M. SUMOylation regulates kainate-receptor-mediated synaptic transmission. *Nature* **447**, 321–325 (2007).
- Maraschi, A. *et al.* Parkin regulates kainate receptors by interacting with the GluK2 subunit. *Nat. Commun.* **5**, 5182 (2014).
- Selak, S. *et al.* A role for SNAP25 in internalization of kainate receptors and synaptic plasticity. *Neuron* **63**, 357–371 (2009).
- Chamberlain, S. E. L. *et al.* SUMOylation and phosphorylation of GluK2 regulate kainate receptor trafficking and synaptic plasticity. *Nat. Neurosci.* **15**, 845–852 (2012).
- Suzuki, E. & Kamiya, H. PSD-95 regulates synaptic kainate receptors at mouse hippocampal mossy fiber-CA3 synapses. *Neurosci. Res.* **107**, 14–19 (2016).
- Basu, R., Taylor, M. R. & Williams, M. E. The classic cadherins in synaptic specificity. *Cell. Adh. Migr.* **9**, 193–201 (2015).
- Saglietti, L. *et al.* Extracellular interactions between GluR2 and N-cadherin in spine regulation. *Neuron* **54**, 461–477 (2007).
- Nuriya, M. & Haganir, R. L. Regulation of AMPA receptor trafficking by N-cadherin. *J. Neurochem.* **97**, 652–661 (2006).
- Fannon, A. M. & Colman, D. R. A model for central synaptic junctional complex formation based on the differential adhesive specificities of the cadherins. *Neuron* **17**, 423–434 (1996).

59. Epsztein, J., Represa, A., Jorquera, I., Ben-Ari, Y. & Crépel, V. Recurrent mossy fibers establish aberrant kainate receptor-operated synapses on granule cells from epileptic rats. *J. Neurosci.* **25**, 8229–8239 (2005).
60. Peret, A. *et al.* Contribution of aberrant GluK2-containing kainate receptors to chronic seizures in temporal lobe epilepsy. *Cell Rep.* **8**, 347–354 (2014).
61. Matsuda, K. *et al.* Transsynaptic modulation of kainate receptor functions by Clq-like proteins. *Neuron* **90**, 752–767 (2016).
62. Martin, S., Bouschet, T., Jenkins, E. L., Nishimune, A. & Henley, J. M. Bidirectional regulation of kainate receptor surface expression in hippocampal neurons. *J. Biol. Chem.* **283**, 36435–36440 (2008).
63. Bard, L. *et al.* A molecular clutch between the actin flow and N-cadherin adhesions drives growth cone migration. *J. Neurosci.* **28**, 5879–5890 (2008).
64. Marchal, C. & Mulle, C. Postnatal maturation of mossy fibre excitatory transmission in mouse CA3 pyramidal cells: a potential role for kainate receptors. *J. Physiol. (Lond.)* **561**, 27–37 (2004).
65. Mori, M., Heuss, C., Gähwiler, B. H. & Gerber, U. Fast synaptic transmission mediated by P2X receptors in CA3 pyramidal cells of rat hippocampal slice cultures. *J. Physiol. (Lond.)* **535**, 115–123 (2001).

Acknowledgements

This study was supported by the Centre National de la Recherche Scientifique, the Conseil Régional d'Aquitaine, the European Commission (EIF Fellowship awarded to MC), the Agence Nationale de la Recherche (contract MossyGlu), the labex BRAIN and the Fondation pour la Recherche Médicale (FDT20140931189 to S.F.). We acknowledge Françoise Coussen for fruitful initial discussions and help with the GluK2a plasmids. We thank Séverine Deforges for producing the plasmid DNAs; Elisabeth Normand, Audrey Lacquemant and Amandine Gautier for taking care of the mice; Adam Gorlewicz for help with immunocytochemistry and for discussion on Cadherins; Federico Trigo for help in setting up the uncaging experiments; and Matthieu Sainlos for the help on the production of anti-GFP nanobody. Cellular imaging was in part performed at the Bordeaux Imaging Center, a service unit of the CNRS-INSERM and Bordeaux University, member of the National Infrastructure France BiolImaging.

Author contributions

S.F. performed and analysed slice electrophysiology experiments in combination with pharmacological and molecular replacement approaches with the help of M.C. M.C. initiated the project and developed single-cell electroporation of KAR cDNAs in hippocampal slices. I.C. performed image acquisition and analysis of SEP–GluK2a experiments. O.T. helped design the imaging experiments and contributed to discussion. V.L. helped S.F. to perform image acquisition and analysis. C.M. supervised the project and wrote the manuscript together with S.F. and M.C.

Additional information

Supplementary Information accompanies this paper at <http://www.nature.com/naturecommunications>

Competing financial interests: The authors declare no competing financial interests.

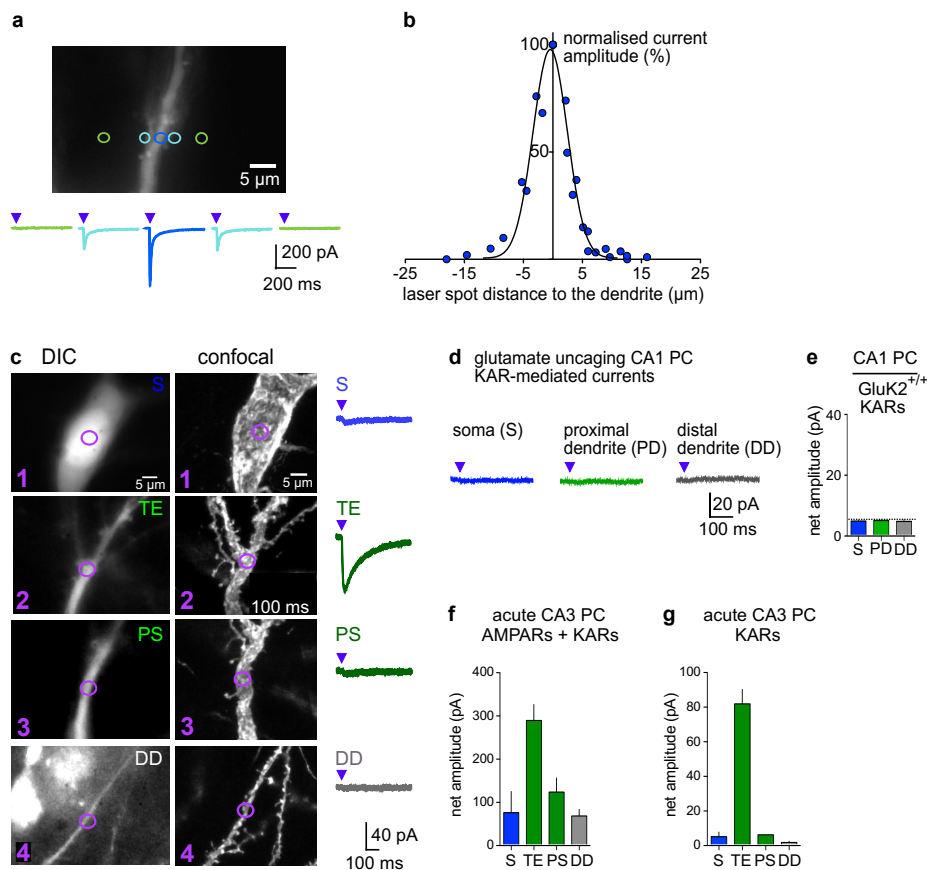
Reprints and permission information is available online at <http://npg.nature.com/reprintsandpermissions/>

How to cite this article: Fièvre, S. *et al.* Molecular determinants for the strictly compartmentalized expression of kainate receptors in CA3 pyramidal cells. *Nat. Commun.* **7**:12738 doi: 10.1038/ncomms12738 (2016).

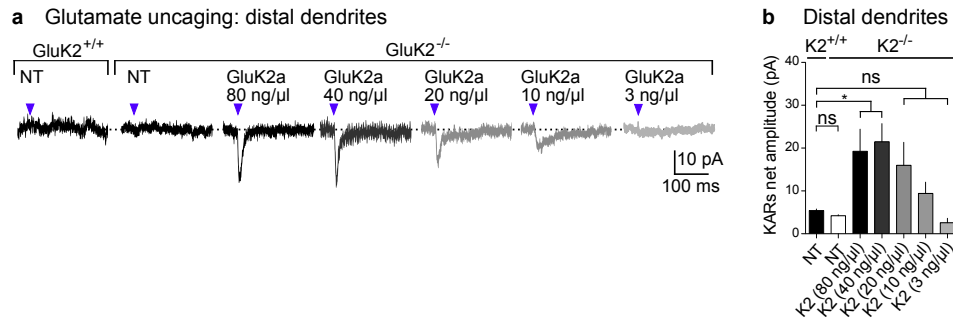


This work is licensed under a Creative Commons Attribution 4.0 International License. The images or other third party material in this article are included in the article's Creative Commons license, unless indicated otherwise in the credit line; if the material is not included under the Creative Commons license, users will need to obtain permission from the license holder to reproduce the material. To view a copy of this license, visit <http://creativecommons.org/licenses/by/4.0/>

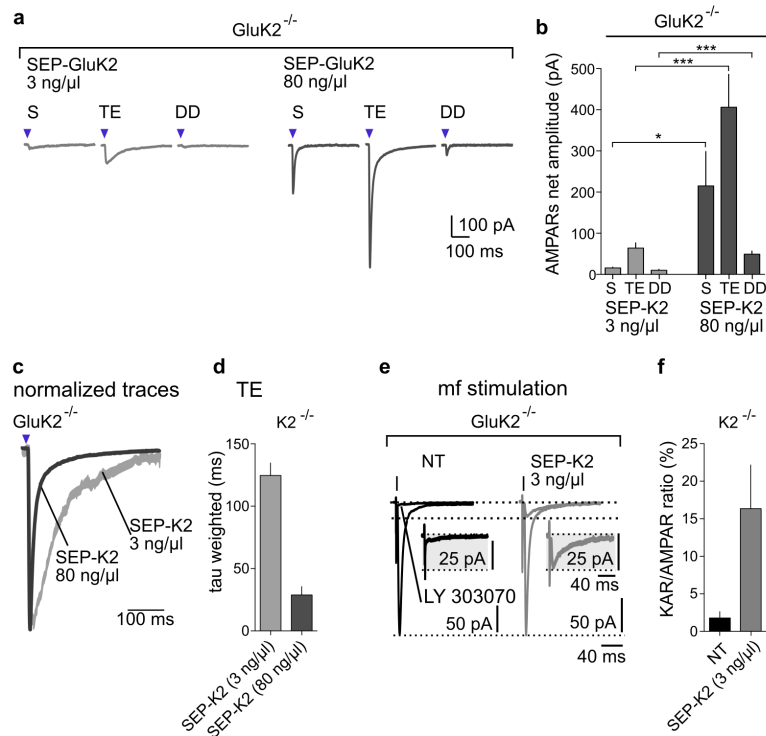
© The Author(s) 2016



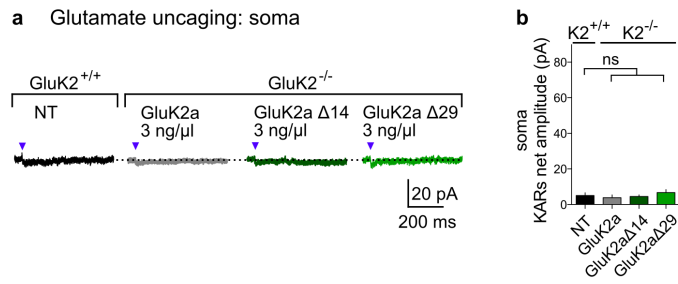
Supplementary Figure 1: Spatial precision of monophoton glutamate uncaging in organotypic slice cultures. **a)** To have access to the spatial precision of glutamate uncaging system, AMPARs-currents were recorded following glutamate uncaging at different distances from a dendrite. **b)** Graph representation of the percentage of current amplitude after uncaging on the dendrite to the current amplitude after uncaging at different distance from the dendrite itself. **c)** Epifluorescence images and corresponding confocal images of a CA3 PC (GluK2^{+/+}) illustrating the location where glutamate uncaging (MNI-glutamate 500 μM) was performed and the corresponding evoked KAR-current (the image of the cell was already used in Figure 1). Purple arrow heads represent the time at which uncaging was done (405 nm, 2 ms). Glutamate uncaging was performed on the soma (S), thorny excrescences (TE), proximal shaft (PS) and distal dendrite (DD). The confocal images were acquired after glutamate uncaging, fixation and mounting of the slice. **d, e)** Sample traces illustrating KAR-currents evoked by glutamate uncaging (in the presence of 25 μM LY303070) in organotypic slices prepared from GluK2^{+/+} mice. Uncaging was performed in different districts of the CA1 PC (soma, proximal dendrite and distal dendrite). Summary bar graph illustrating the average net amplitude of the evoked currents (net amplitude soma: 4.5 ± 0.3 pA; proximal dendrite: 4.7 ± 0.2 pA; distal dendrite: 4.4 ± 0.6 pA; n=5). **f, g)** Bar graph summarizing the average net amplitude of evoked currents after glutamate uncaging in different compartments of CA3 PCs (S, TE, PD, DD) from acute (GluK2^{+/+}) slices in absence of LY303070 (F) in order to record both the AMPAR and KAR component (net amplitude: S: 73.5 pA ± 49.1 pA; TE: 286.7 ± 37.1 pA; PS: 121.2 ± 32.6 pA; DD: 65.7 ± 15.6 pA; n=4) or in presence of LY 303070 (G) in order to record KARs component (net amplitude: S: 4.4 ± 2.7 pA; TE: 81.23 ± 8.3 pA; PS: 5.5 ± 0.0 pA; 1.0 ± 0.7 pA n=4). In all panels, values are presented as mean ± SEM of n experiments.



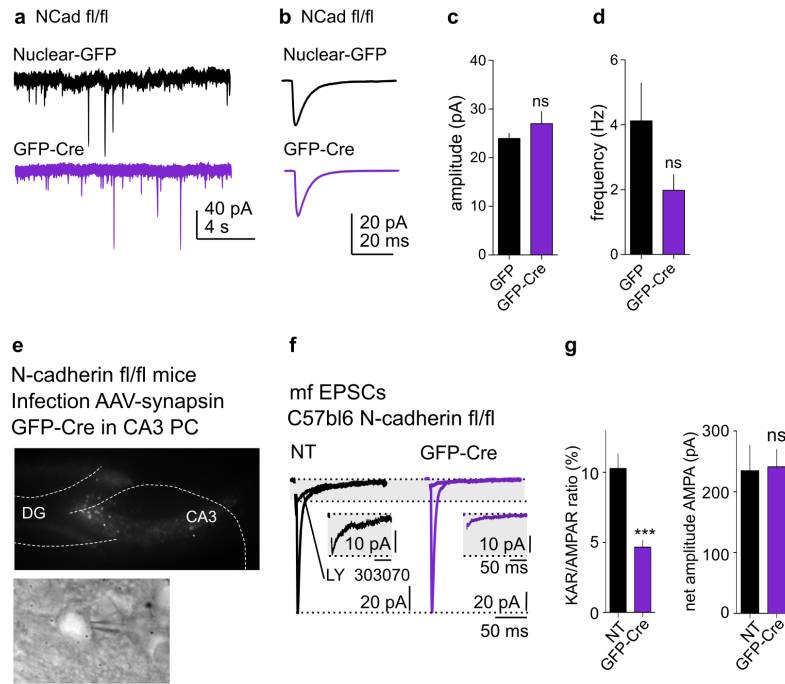
Supplementary Figure 2: Semi-quantitative replacement of KARs. a) Sample traces illustrating the KAR-currents evoked by glutamate uncaging on the distal dendrites CA3 PCs in organotypic slice cultures prepared from GluK2^{+/+} and GluK2^{-/-} not transfected (NT) or transfected with different amount of GluK2a cDNA (80, 40, 20, 10, 3 ng/μl). **b)** Summary bar graphs illustrating the average amplitude of the KARs evoked currents at the distal dendrites (Average net current amplitude: WT: 5.4 ± 0.3 pA; GluK2a 80 ng/μl: 19.2 ± 5.2 pA; GluK2a 40 ng/μl: 21.5 ± 4.2 pA; GluK2a 20 ng/μl: 16.0 ± 5.4 pA; GluK2a 10 ng/μl: 9.4 ± 2.6 pA; GluK2a 3 ng/μl: 2.6 ± 1.0 pA). In all panels, values are presented as mean ± SEM of n experiments. Data were compared using one way ANOVA followed by Dunnett's multiple comparison test (ns p>0.05, *p<0.05).



Supplementary Figure 3: Rescue of KAR-currents with GluK2a-SEP. **a)** Sample traces illustrating KAR-currents evoked by glutamate uncaging in different districts of CA3 PCs (S, TE and DD) in organotypic slice cultures prepared from GluK2^{-/-} mice and transfected with either 3ng/μl or 80 ng/μl of GluK2a-SEP cDNA. **b)** Summary bar graphs illustrating the average amplitude of KAR-currents illustrated in (a). GluK2a-Sep 3 ng/μl; S, 17.1 ± 2.3 pA; TE, 63.9 ± 12.7 pA; DD, 9.7 ± 2.6 pA, experiments performed on 6-7 cells, 4 slices and 3 mice. GluK2a-Sep 80 ng/μl; mean amplitude, soma, 216.5 ± 83.6 pA; TE, 406.3 ± 80.2 pA; DD, 49.4 ± 7.5 pA; experiments performed on 5-6 cells, 4 slices and 3 mice. **c, d)** Sample traces of KAR-currents evoked by glutamate uncaging showed in a, and scaled at the peak illustrating differences in the decay between SEP-GluK2a transfected at 3 ng/μl or 80 ng/μl. Quantification of the decay rate (tau weighted) of KAR-currents evoked onto TE by glutamate uncaging for SEP-GluK2a transfected at 3 ng/μl (mean tau weighted, 28.8 ± 6.7 ms, n = 7) or 80 ng/μl (mean tau weighted, 124.7 ± 9.9 ms, n = 6). **e, f)** Sample traces illustrating synaptic currents evoked by mf stimulation in organotypic slices prepared from GluK2^{-/-} mice, not transfected (NT) or transfected with SEP-GluK2a cDNA 3 ng/μl. Experiments were performed in the presence of bicuculline (10 μM), D-AP5 (50 μM) and NBQX (150 nM). Traces represent the average synaptic currents evoked at 3 Hz in the absence and in the presence of 25 μM LY303070, to isolate the AMPAR and the KAR component, respectively. In the insert are showed enlargements, by the same proportion, of isolated KAR-EPSCs. Bar graph summarizing the KAR/AMPA ratio obtained from the experiments presented in e. GluK2^{-/-} NT: 1.7 ± 0.8 %, experiment performed on 3 cells, 3 slices and 2 mice; 3 ng/μl: 16.35 ± 5.8 %, experiment performed on 6 cells, 6 slices and 3 mice. In all panels, values are presented as mean ± SEM of n experiments. Data were compared using unpaired t-test (ns p>0.05, *p<0.05, ***p<0.001).



Supplementary Figure 4: Glutamate uncaging on the soma after reexpression of CTD truncated GluK2 subunits. **a)** Sample traces illustrating the KAR-currents evoked by glutamate uncaging on soma of CA3 PCs in organotypic slice cultures prepared from GluK2^{+/+} and GluK2^{-/-} not transfected (NT) or transfected with 3 ng/μl of wt or mutated GluK2a cDNA (Δ14 and Δ29). **b)** Summary bar graphs illustrating the average amplitude of the KARs evoked currents presented in (A) (Average net current amplitude: WT: 5.0 ± 1.6 pA; GluK2a: 3.8 ± 1.6 pA; GluK2a Δ14: 4.5 ± 0.9 pA; GluK2a Δ29: 6.7 ± 1.7 pA; GluK2^{-/-}, not transfected 1.0 ± 0.1 pA n=7-10). Values are presented as mean ± SEM of n experiments. Data were compared using one way ANOVA followed by Dunnett's multiple comparison test (ns p>0.05).



Supplementary Figure 5: Effect of N-cadherin knockout on mEPSCs in organotypic cultures; *in vivo* knockout of N-Cadherin in CA3 PC decreases the amount of KARs at mf-CA3 synapse. **a, b)** Sample traces illustrating mEPSCs recorded from CA3 PCs in organotypic slice cultures prepared from NCad^{fl/fl} mice electroporated either with nuclear-GFP or GFP-Cre. Experiments were performed -70 mV, in the presence of TTX, bicuculline and AP5 at 34 °C. **c, d)** Bar graphs summarizing the average amplitude and frequency of mEPSCs from experiments presented in (a) and (b). Nuclear-GFP, mean amplitude, 23.9 ± 1.1 pA; mean frequency, 4.1 ± 1.1 Hz; Experiment performed on 6 cells, 4 slices and 3 mice. GFP-Cre, mean amplitude, 26.9 ± 2.5 pA; mean frequency, 1.9 ± 0.5 Hz; Experiment performed on 6 cells, 4 slices and 3 mice. **e)** Representative hippocampal acute slice from N-Cadherin^{fl/fl} mice infected in the CA3 region with an AAV2.9 encoding GFP-cre. Slices were prepared 3-4 weeks after infection. **f)** Sample traces illustrating synaptic currents evoked by mf stimulation in CA3 PCs from acute slices prepared from N-Cadherin^{fl/fl} mice not transfected (NT) or infected with GFP-Cre (for clarity stimulus artifacts were removed). Experiments were carried in the presence of bicuculline (10 μM), D-AP5 (50 μM) and NBQX (150 nM). Traces represent the average of synaptic currents evoked at 3 Hz in the absence and in the presence of 25 μM LY303070, to isolate the AMPAR and the KAR component, respectively. In the insert are showed enlargements, by the same proportion, of isolated KAR-EPSCs. **g)** Summary bar graphs illustrating the KAR/AMPA and the amplitude of the AMPAR EPSCs obtained from the experiments presented in B. (mean KAR/AMPA ratio: not transfected: 10.3 ± 1.0 %; GFP-cre: 4.7 ± 0.5 %; n=13; mean amplitude: not transfected: 234.6 ± 42.4 pA; GFP-cre: 241.0 ± 28.9 pA; n=13). In all panels, values are presented as mean ± SEM of n experiments. Data were compared using unpaired t-test (ns p>0.05, **p<0.01).